Dendritic Cell – Fibroblast Crosstalk via TLR9 and AHR Signaling Drives Lung Fibrogenesis

Hannah Carter [1], Rita Medina Costa [1], Taylor S. Adams [2], Talon Gilchrist [1], Claire E. Emch [1], Monica Bame [1], Justin M. Oldham [3], Angela L. Linderholm [4], Imre Noth [5], Naftali Kaminski [2], Bethany B. Moore [1,3], Stephen J. Gurczynski* [1].

1) Department of Microbiology and Immunology, University of Michigan, Ann Arbor, MI
2) Section of Pulmonary, Critical Care and Sleep Medicine, Yale University School of Medicine, New Haven, Connecticut, USA.
3) Division of Pulmonary and Critical Care Medicine, University of Michigan, Ann Arbor, MI
4) Division of Pulmonary and Critical Care Medicine, University of California, Davis, California.
5) Division of Pulmonary and Critical Care Medicine, University of Virginia, Charlottesville, Virginia.

* Corresponding author:

Stephen J. Gurczynski, PhD

5608C Medical Science II

1137 Catherine St

Ann Arbor, MI 48109-2200

sgurczyn@umich.edu

(734) 647-9968 phone

(734)615-2331 fax

The Authors declare no conflicts of interest.

Funding sources. This work was funded by NIH R35 HL144481 awarded to BBM, T32GM007863 awarded to HC, and a Boehringer Ingelheim discovery award in ILD. This work was made possible by the Pulmonary Fibrosis Foundation, by an independent grant from Boehringer Ingelheim Pharmaceuticals, Inc. who provided the financial support. The authors meet criteria for authorship as recommended by the International Committee of Medical Journal Editors (ICMJE) and were fully responsible for all aspects of the trial and publication development.

Author contributions. HC performed experiments, analyzed data, wrote, and edited the manuscript. TSA analyzed and interpreted data. RMC, TG, CE, and MB performed experiments and analyzed data. JMO, ALL, and IN provided clinical data. BBM analyzed and interpreted data and edited the manuscript. SJG wrote and edited the manuscript as well as analyzing and interpreting data.

Word count: 5387

Abstract

Idiopathic pulmonary fibrosis (IPF) is characterized by progressive scarring and loss of lung function. With limited treatment options, patients succumb to the disease within 2-5 years. The molecular pathogenesis of IPF regarding the immunologic changes that occur is poorly understood. We characterize a role for non-canonical aryl-hydrocarbon receptor signaling (ncAHR) in dendritic cells (DCs) that leads to production of IL-6 and IL-17, promoting fibrosis. TLR9 signaling in myofibroblasts is shown to regulate production of TDO2 which converts tryptophan into the endogenous AHR ligand kynurenine. Mice with augmented ncAHR signaling were created by crossing floxed AHR exon-2 deletion mice ($AHR_{\Delta ex2}$) with mice harboring a CD11c-Cre. Bleomycin was used to study fibrotic pathogenesis. Isolated CD11c+ cells and primary fibroblasts were treated ex-vivo with relevant TLR agonists and AHR modulating compounds to study how AHR signaling influenced inflammatory cytokine production. Human datasets were also interrogated. Inhibition of all AHR signaling rescued fibrosis, however, $AHR_{\Delta ex2}$ mice treated with bleomycin developed more fibrosis and DCs from these mice were hyperinflammatory and profibrotic upon adoptive transfer. Treatment of fibrotic fibroblasts with TLR9 agonist increased expression of TDO2. Study of human samples corroborate the relevance of these findings in IPF patients. We also, for the first time, identify that AHR exon-2 floxed mice retain capacity for ncAHR signaling.

Abstract word count 211

Introduction

Idiopathic Pulmonary Fibrosis (IPF) is a progressive, fibrotic disease with estimated survival of 2-5 years after diagnosis. Risk factors include male sex, cigarette smoking, repeated viral infection, with median age at diagnosis of 66 years.(1) Treatments slow progressive fibrosis, but only lung transplant is curative.(2) Fibroblast activation and excess production of collagens are critical factors that underlie disease progression, however, fibrogenesis is a complex and poorly understood process requiring cooperation / crosstalk between multiple cell subsets. Myriad inflammatory cells accumulate in fibrotic lungs including dendritic cells (DCs), macrophages, and lymphocytes, however, the ultimate role of the immune system in initiation and progression of fibrosis is not understood. Immune responses may promote progressive scarring but treating patients with steroids is counterintuitively harmful highlighting the need for more research into the interactions between immune cell populations and fibrogenesis.(3) We have previously defined an important role for tissue resident DCs, and more specifically DCs expressing the aryl-hydrocarbon receptor (AHR) in viral-mediated pulmonary fibrosis following bone marrow transplantation.(4, 5) Tissue resident DCs have been shown to accumulate in the lungs of both IPF patients and bleomycin treated mice, however their exact role in the initiation or progression of pulmonary fibrosis is unclear. (6-8)

The canonical Aryl-Hydrocarbon Receptor (AHR) pathway is an intracellular signaling cascade originally described as the major sensor of a poly-cyclic aromatic hydrocarbon (PAH) toxicants, e.g., dioxin.(9) More recently, endogenous AHR ligands such as the kynurenine family of tryptophan metabolites have been described.(10, 11) Kynurenine can be made by indoleamine-2,3-dioxygenase (IDO) or tryptophan 2,3-dioxygenase (TDO), and kynurenine / tryptophan ratios are increased in patients with fibrotic lung disease.(12) Increased kynurenine / tryptophan ratios in the blood are also prognostic indicators for many inflammatory lung diseases, including cancers and SARS-CoV-2.(13-18)

AHR is constitutively expressed in an inactive form sequestered in the cytoplasm bound to various chaperone proteins.(19) Binding of ligand exposes a nuclear localization signal which facilitates translocation of AHR to the nucleus wherein the chaperone coat is recycled and AHR dimerizes with its major canonical partner ARNT.(20, 21) This AHR / ARNT dimer binds to xenobiotic response elements in the genome and activates transcription of a variety of gene products including the CYP family of cytochrome p450 oxidases.(22)

102 AHR is present and involved in inflammation in several lung cell types including immune
103 cells such as DCs, macrophages, and lymphocytes as well as structural cells such as epithelial
104 cells and fibroblasts. Recently AHR has been studied for its interactions with other binding
105 partners outside of ARNT, i.e., NFkB subunits RelA / RelB and KLF6, in what is termed "non-
106 canonical AHR signaling" (ncAHR) which is especially important in regulating expression of pro-
107 inflammatory cytokines in immune cells like dendritic cells (DCs) and macrophages.(4, 23-25)
108 Production of pro-inflammatory cytokines by DCs is augmented in the presence of AHR ligands
109 suggesting a role for AHR in concert with NFkB when triggered by pro-inflammatory signals.(26,
110 27) AHR and TLR signaling, especially TLR9, have also been studied separately for their ability
111 to promote fibrogenesis by directly augmenting fibroblast differentiation into pro-fibrotic
112 myofibroblasts.(28, 29) Pro-inflammatory TLR9 / AHR responsiveness has been linked to
113 worsened IPF progression(30), however, the functional binding partners of AHR in inflammatory
114 vs normal conditions, the triggers which divert AHR from its canonical pathway, and the exact
115 role of AHR in complex pathologies such as fibrosis are not well understood.

116 Here, we present data that ncAHR signaling is an important modulator of DC immune
117 responses during the progression of pulmonary fibrosis. Using the bleomycin mouse model of
118 pulmonary fibrosis, we demonstrate that AHR+ DCs accumulate in the lungs and drive
119 production of IL-6 in an AHR dependent fashion. AHR plays a role in differentiation of several
120 immune cells, including Treg, Th-17 and Th-22 cells(31-33), which makes whole-body knock
121 outs non-ideal for studying immune responses. Using a DC-specific deletion of the DNA binding
122 region of AHR (CD11c-Cre / $AHR_{\Delta ex2}$), we further demonstrate deletion of canonical AHR
123 function in DCs leads to significant upregulation of ncAHR signaling, pro-inflammatory cytokines
124 and worsened fibrosis in the bleomycin model. This work also demonstrated that adoptive
125 transfer of ncAHR-activated DCs can promote fibrogenesis in a CD4 T cell-independent
126 manner, highlighting an unappreciated role for DCs in fibrogenesis. We also provide evidence
127 that myofibroblasts in the lungs of both IPF patients and fibrotic mice express the enzymes that
128 convert tryptophan into endogenous AHR ligands highlighting an important role for TDO2
129 specifically in the fibrogenic circuit that is established between structural cells and immune cells
130 in the fibrotic lung.

131 **Materials and Methods**

132 **Mouse line, cell lines, and reagents.** All experiments were conducted under an IACUC
133 approved animal protocol. WT C57Bl/6J mice were ordered from Jackson labs and used
134 between 6-8 weeks of age. $AHR_{\Delta ex2}$ mice were generated by crossing the AHR^{fx} line

135 (Ahrtm3.1Bra/J, strain 6203, Jackson labs) with a CD11c-Cre expressing line (B6.Cg-Tg(Itgax-
136 cre)1-1Reiz/J, strain 8068, Jackson labs). Resulting pups were verified to contain both Cre and
137 the AHR floxed alleles via PCR using Jackson labs recommended primers. CD11c+ cells were
138 further verified to contain the AHR exon2 excised allele via PCR using Jackson labs
139 recommended primers. $AHR_{\Delta ex2}$ mice were bred at the University of Michigan mouse breeding
140 facility and used between 6-8 weeks of age. For some experiments AHR^{fx} mice which did not
141 express CD11c-Cre were used as littermate controls. Bleomycin was purchased as Blenoxane
142 from the pharmacy at the University of Michigan hospital, 1U/mL stocks were made using sterile
143 saline and mice were administered 0.75U/kg via the oral-pharyngeal route. The AHR and TDO2
144 inhibitors CH223191 and 680C91 (Tocris) were used at 5 mg/kg and 15mg/kg respectively for *in*
145 *vivo* experiments, CH223191 was used between 10-30 μM for *in vitro* treatment of cell culture.
146 The TiPARP (PARP7) inhibitor RBN2397 (Selleckchem) was used at a concentration of 10 μM.
147 The TLR9 agonist ODN2395 (Invivogen) was used between 0.1 – 1.0 μM.

148 **Generation of inducible iCD103+ DCs.** Inducible CD103 (iCD103) DCs were generated from
149 mouse bone marrow as previously described.(4, 34) In short, bone marrow cells were
150 aseptically isolated from the femurs of indicated mouse lines and incubated for 16-days in RPMI
151 media containing 10% heat inactivated FBS, 1% Pen/Strep cocktail, 50μM β-mercapto-ethanol,
152 3 ng/mL GMCSF (R&D systems) and 200 ng/mL Flt3-L (R&D systems) before any additional
153 treatment. iCD103 cells were characterized to be CD11c+, MHCII+, and CD103+ by flow
154 cytometry. For adoptive transfer experiments, Groups of WT-B6 mice were first administered
155 BLM before receiving $1x10^6$ iCD103+ cells from $AHR_{\Delta ex2}$ mice via tail vein injection. CD4 T-cell
156 depletion was carried out via i.p. injection of 100 μg anti-CD4 depleting antibody (clone GK1.5
157 Bioxcell) at 0- and 7-days post BLM instillation.(35)

158 **Fibroblast isolation.** Groups of mice were administered BLM or saline as control. 21-days post
159 BLM, lungs were harvested and minced with scissors. Minced lungs were incubated in complete
160 DMEM (DMEM + 10% FBS and 1% pen/strep cocktail) for 7 days to let fibroblasts adhere.
161 Media was changed at 7 days and every 2 days afterwards. Cells were trypsonized and plated
162 on day 14-post isolation for subsequent assays.

163 **Single Cell RNA-seq analysis.** Processed gene expression data from Habermann et al.(36)
164 was downloaded from GSE135893. Raw sequencing data from Adams et al.(37) was
165 downloaded from GSE136831 for reprocessing. Read 2 poly(A) and template-switch oligo
166 contaminants were trimmed using cutadapt (version 3.1). Reads were aligned to genome
167 GRCh38 with STAR (version 2.7.8a) using Gencode annotation release 38.

168 Control and IPF cells previously classified as stromal were filtered from each dataset and
169 combined in R (version 4.0.3) using the library Seurat (version 4.3.0.1). For normalization, raw
170 expression counts were scaled to 10,000 transcripts per cell then natural log transformed with a
171 pseudocount of 1. Cells were split by dataset and integrated using Seurat's reciprocal principal
172 component analysis (RPCA) implementation, followed by dimension reduction, graph
173 embedding, high granularity clustering and cell type re-annotation. These steps were performed
174 iteratively until all multiplets were identified and removed.

175 Of the filtered data presented: Habermann et al. consists of 2,801 cells from 10 controls and 12
176 IPF lungs; Adams et al. consists of 6,850 cells from 26 control and 32 IPF lungs. Integrated
177 gene expression values were only used for PCA-based graph embedding; cluster interrogation
178 and subsequent visualizations were performed with normalized, empirical values. For the
179 heatmap, normalized gene expression values of each cell type were averaged for each subject
180 with 3 or more respective cells. To avoid batch effect between datasets when visualizing gene
181 expression, normalized expression values were further min-max normalized across cells within
182 each dataset.

183 **Generation of single cell suspensions and flow cytometry.** Single cells suspensions were
184 generated via collagenase digestion of lung tissue as previously described.(38) In short, mouse
185 lungs were first perfused via injection of 3-5mL of saline through the right ventricle of the heart.
186 Lungs were resected and minced with scissors before incubation in a collagenase buffer
187 containing 1 mg/mL Collagenase-A (Roche), 2000U DNaseI (Sigma), in complete DMEM media
188 supplemented with 10% heat inactivated FBS and 1% Pen/Strep cocktail for 45 minutes at 37°C
189 in a shaking incubator. Cell suspensions were disrupted by drawing through a 10 mL syringe
190 before filtration through a 100 µm pore sized cell strainer. Resulting single cell suspensions
191 were assayed for cell viability via trypan blue exclusion, staining for flow cytometry was
192 subsequently carried out via incubation with appropriately diluted fluorophore conjugated
193 antibodies. Antibodies used for flow cytometry were as follows: Myeloid flow cytometry staining
194 panel, BV650-CD11b (clone M1/70), BV510-CD45 (clone 30-F11), BV421-I-Ab (MHCII clone
195 AF6-120.1), APC-Cy7-SiglecF (clone E50-2440), APC-Ly6G (clone 1A8) purchased form BD
196 Horizon. BV605-CD64 (clone X54-5/7.1), PerCP-Cy5.5-CD24 (clone M1/69), PE-Cy7-Ly6C
197 (clone HK1.4), PE-CD193 (CCR3 clone J073E5) purchased from Biolegend. PE-eFluor610-
198 CD11c (clone N418), PE-AHR (clone 4MEJJ) purchased from eBioscience. Lymphocyte flow
199 cytometry staining panel. PE-Cy7-IFNγ (clone XMG1.2), FITC-CD3 (clone 17A2) purchased
200 from BD bioscience. APC-Cy7-IL17A (clone TC11-18H10.1), BV570-CD8a (clone 53-6.7),

201 AF700-CD90.2 (Thy1.2 clone 30-H12), BV510-CD4 (clone GK1.5) purchased from Biolegend.
202 PE-eFluor 610-FoxP3 (clone FJK-16s) purchased from eBioscience. Note: Some markers were
203 stained for but were not included in this study. Flow analysis was carried out in FlowJo v. 10.5.

204 **Quantification of collagen via hydroxyproline assay.** Collagen was quantified as described
205 in(39). In short, lungs from BLM or WT mice were resected at the indicated timepoints and
206 homogenized in a buffer of PBS and complete protease inhibitor (Roche). Lung homogenates
207 were diluted 1:1 with 12N hydrochloric acid and incubated overnight at 120°C in well-sealed
208 glass tubes. The following day, aliquots of acid-hydrolyzed lung homogenate were incubated
209 with a chloramine-T solution and then reacted with 4-(Dimethylamino)benzaldehyde.
210 Hydroxyproline was detected via absorbance at 560 nM on a synergy H1 spectrophotometer
211 (Biotek).

212 **Isolation of RNA for qRT-PCR.** RNA was purified from lung tissue or cell pellets via incubation
213 with Trizol reagent following manufacturer directions. RNA quantity and purity was assessed on
214 a nanodrop spectrophotometer (Thermo). Transcript expression was analyzed via reverse
215 transcriptase quantitative real-time PCR using Lunaprobe reagent (New England Biolabs) on a
216 Quantstudio3 thermocycler (ABI). Expression analysis was conducted using a ΔΔct calculation.
217 Transcripts were normalized to expression level of a housekeeping gene, RPL38, using a pre-
218 validated primer probe set (Integrated DNA technologies, Hs.PT.58.40595235.gs). Other primer
219 and probe sequences are detailed in Table 1.

220 **Analysis of plasma concentrations of IL-6 and IL-17 isoforms.** Circulating plasma
221 concentration for IL6 and IL17 (a, c, d and f isoforms) was determined used the Olink (Uppsala,
222 Sweden) Explore platform, which uses proximity extension assays to generate semi-quantitative
223 protein data, which are Log2 transformed for modeling. The association between plasma
224 biomarker concentration and three-year transplant-free survival was assessed in a combined
225 cohort of patients with IPF (n=366) from the University of Virginia, University of Chicago and
226 University of California at Davis using univariable Cox proportional hazards regression [IRB
227 approval and subject characteristics were previously reported(40)]. Survival was plotted for each
228 quartile of IL6 concentration using the Kaplan-Meier estimator. The proportional hazards
229 assumption was checked and satisfied for each biomarker tested.

230 **Statistical analysis.** Statistical analysis was conducted in Graphpad Prism v.9.1.0. Statistical
231 significance was determined using students T-test when two groups were compared and

232 ANOVA using Holm-Sidak's post-test when three or more groups were compared. Relevant
233 statistical information, i.e., P-values and n-values, are given in individual figure legends.

234 **Results**

235 **CD103+ DCs accumulate in the fibrotic lung, promote fibrogenesis and show evidence of**
236 **pro-inflammatory AHR signaling.** We previously published that AHR+ CD103+ DCs were
237 recruited to lungs, and drove lung injury and fibrosis following bone marrow transplantation and
238 herpesvirus infection(4); however, a pathogenic role for AHR and DCs in non-infectious forms of
239 pulmonary fibrosis is not known. To address this, we characterized lung DCs using a bleomycin
240 model of pulmonary fibrosis. Lung leukocytes were analyzed via flow cytometry at 7- and 14-
241 days post-treatment and a significant increase in CD103+ DCs (CD45+, CD11c+, MHCII +,
242 CD103+, CD11b-) was noted at both time points (Fig. 1A). Differentiation of CD103+ DCs
243 requires the transcription factor BATF3 and CD103+ DCs are completely absent in BATF3$^{-/-}$
244 mice.(41) To clarify the role of lung CD103+ DCs in mediating fibrogenesis we treated BATF3$^{-/-}$
245 mice with bleomycin for 14-21 days and verified the absence of CD103+ DCs in the lung by flow
246 cytometry (Fig. 1B). BATF3$^{-/-}$ mice exhibited durable protection from bleomycin induced
247 pulmonary fibrosis exhibiting less collagen production at 14 days as assessed by hydroxyproline
248 assay and at 21-days as assessed by qRT-PCR for collagen I transcript (Fig. 1C and 1D).
249 Interestingly, BATF3$^{-/-}$ mice also displayed less IL-6 transcript indicating that CD103+ DCs are
250 important regulators of pro-inflammatory / fibrotic cytokine production following bleomycin
251 challenge (Fig. 1E). We next analyzed expression of AHR in various lung immune cells via flow
252 cytometry at 7-days post bleomycin treatment (markers for cell subsets are detailed in Sup.
253 Table 1). The highest percentage of AHR+ cells was found in CD103+ DCs (cDC1s ~60%)
254 while most other immune cells had AHR+ rates between 3-5% (Fig. 1F). To further verify that
255 expression of AHR was augmented in lung DCs we isolated CD11c+ cells via magnetic bead
256 isolation from the lungs of bleomycin treated or control mice. CD11c+ cells from the lungs of
257 bleomycin treated mice had increased expression of AHR in comparison to control mice but
258 interestingly had decreased expression of the canonical AHR gene product Cyp1b1 (Fig. 1G
259 and 1H). In agreement with our previous data using BATF3$^{-/-}$ mice, CD11c+ cells isolated from
260 bleomycin treated mice had increased expression of IL-6 further indicating that lung DCs are an
261 important source of pro-inflammatory cytokines (Fig. 1I).

262 **Production of AHR ligands is augmented during BLM-induced fibrosis and complete AHR**
263 **inhibition ameliorates disease.** Several endogenous ligands for AHR have been described,
264 most notably, kynurenine which is a metabolite of tryptophan processed by the heme-dependent

265 oxygenases IDO1/2 and TDO2.(42) Whole lung homogenates were prepared from saline-
266 treated or BLM-instilled mice. Concentrations of lung-associated kynurenine were assayed via
267 ELISA. A significant increase in lung-associated kynurenine was observed at both 7- and 14-
268 days post-BLM (Fig. 2A). These data suggest activation of AHR signaling in the fibrotic lung
269 may promote development of BLM-induced fibrosis. To test this hypothesis, we administered
270 the complete AHR inhibitor, CH223191, following BLM instillation. Complete inhibition of AHR
271 signaling ameliorated development of bleomycin-induced pulmonary fibrosis. Mice treated with
272 CH223191 exhibited less collagen deposition than non-treated mice (Fig. 2B) and had
273 decreased evidence of fibrotic pathology on trichrome stained lung sections (Fig. 2C).

274 **Deletion of the AHR DNA binding domain reduces canonical AHR signaling in DCs but**
275 **AHR expression is retained and augments inflammatory non-canonical AHR signaling.** To
276 further address AHR signaling in lung DCs we bred mice that harbored floxed copies of AHR
277 exon-2 (43) crossed to a strain that harbored Cre recombinase under control of the CD11c
278 promoter (CD11c-AHR$_{\Delta ex2}$ mice referred to as AHR$_{\Delta ex2}$, Fig. 3A). Previous reports using these
279 AHR exon-2 floxed mice described them as AHR-null mutants (43); however, we identified an
280 alternative start codon (Supplemental Fig. 1A red text) that is introduced as part of the fusion of
281 AHR exon-1 and exon-3 resulting in a 14 amino acid N-terminal leader sequence (Supplemental
282 Fig. 1A green text) fused in frame to AHR exons 3 – 10 (Supplemental Fig. 1A blue text). DCs
283 generated from these mice are indeed null for production of canonical AHR response genes
284 following stimulation with kynurenine (Fig. 3B), however, primers specific for AHR exon3-4
285 showed no difference in the amounts of AHR transcript while primers specific for the junction of
286 exon1-2 showed a significant reduction in AHR$_{\Delta ex2}$ mice (Fig. 3C). Furthermore, AHR was still
287 detectable in CD103+ DCs produced from AHR$_{\Delta ex2}$ mice as assessed by intracellular flow
288 cytometry (Fig. 3D and 3E).

289 We next generated cDNA from BMDCs isolated from either heterozygous B6 / AHR$_{\Delta ex2}$ or
290 homozygous AHR$_{\Delta ex2}$ mice. PCR of the AHR ORF produced two bands in the heterozygous
291 mice of approximately 2400 and 2200 bp (Supplemental Fig. 1B) corresponding to the predicted
292 sizes of the full length AHR or AHR$_{\Delta ex2}$ ORF, respectively, and a single band of approximately
293 2200bp in the AHR$_{\Delta ex2}$ mice. We cloned these products into pI-Cherry-NEO vector which co-
294 expressed each construct with mCherry and verified sequences of both full length and AHR$_{\Delta ex2}$
295 PCR products via sanger sequencing (data not shown) . To verify the specificity of the AHR flow
296 cytometry antibody, We conducted flow cytometry on 3T3 cells transfected with either AHR full
297 length or AHR$_{\Delta ex2}$ constructs and noted ~30% of cells expressed mCherry after 48 hours

298 (Supplemental Fig. 1C). We also examined expression of AHR in these transfected cells and
299 noted a ~2-fold increase in AHR MFI in both full length and $AHR_{\Delta ex2}$ transfections indicating both
300 constructs produced an in frame AHR protein. Thus, we now report that although canonical
301 AHR signaling is ablated following excision of exon-2, a truncated AHR protein is produced that
302 likely mediates effects through the ncAHR pathway.

303 To assess impact of DC AHR signaling on development of fibrosis we administered BLM to
304 groups of WT B6 or $AHR_{\Delta ex2}$ mice. $AHR_{\Delta ex2}$ mice exhibited increased fibrosis and ~1.5-fold
305 increased collagen deposition 21-days post BLM versus WT mice (Fig. 3F and 3G). We were
306 surprised by this result as complete AHR inhibition ameliorated fibrosis (Fig. 1C). We next
307 administered CH223191 to groups of BLM-treated WT or $AHR_{\Delta ex2}$ mice. Interestingly, complete
308 inhibition of AHR was still ameliorative (Fig. 3F) indicating that, while deletion of AHR exon-2
309 effectively ablated canonical AHR signaling in CD11c+ cells (Fig 3B), ncAHR signaling was
310 likely still functional and could mediate pro-fibrotic effects.

311 **Loss of canonical AHR signaling in CD11c+ cells exacerbates fibrosis via a ncAHR-**
312 **dependent mechanism.** To further test the role AHR in CD103+ DCs we generated pure
313 populations of induced CD103+ DCs (iCD103) from bone marrow stem cells.(34) We previously
314 published iCD103 DCs express many cDC1 markers and express AHR.(4) We addressed the
315 role of CD103+ DCs in mediating fibrosis by adoptively transferring iCD103+ DCs from $AHR_{\Delta ex2}$
316 mice into groups of BLM treated WT mice. Lungs were harvested at 21-days post BLM and
317 collagen content was assessed via hydroxyproline assay. B6 BLM treated mice that had
318 received an adoptive transfer of $AHR_{\Delta ex2}$ iCD103+ cells developed increased fibrosis exhibiting
319 significantly increased lung collagen over mice receiving a sham transfer (Fig. 4A). We also
320 administered neutralizing αCD4 antibody to BLM-treated mice with $AHR_{\Delta ex2}$ iCD103+ adoptive
321 transfer, however, no change in fibrosis was observed indicating the pro-fibrotic effects of
322 $AHR_{\Delta ex2}$ CD11c+ cells are independent of CD4+ T-cells(Fig. 4A).

323 The role of AHR in modulating cytokine responses is complex. Genes such as TiPARP
324 induced through the canonical AHR pathway downregulate cytokine and interferon responses
325 through post-translational modification of critical kinases such as TBK1 thus shutting down
326 NFκB and IRF responses.(44-47) In contrast, AHR itself can directly bind NFκB and drive pro-
327 inflammatory cytokine responses.(27, 48-50) Multiple TLRs, including TLR9, have been
328 implicated in the progression of pulmonary fibrosis.(29, 51, 52) To address if DC IL-6 expression
329 was dependent on cooperation between AHR and TLR signaling, we stimulated iCD103 DCs
330 with the TLR9 agonist ODN2395. Cells generated from $AHR_{\Delta ex2}$ mice expressed over 2-fold

331 more IL-6 in comparison to ODN2395-treated iCD103 cells from WT mice (Fig. 4B).
332 Interestingly, while ODN treatment could stimulate expression of TiPARP in WT iCD103 DCs,
333 this effect was abrogated in $AHR_{\Delta ex2}$ iCD103 DCs (Fig 4C). Together, these data indicate
334 expression of TiPARP is dependent on canonical AHR signaling while expression of IL-6 is
335 augmented by ncAHR signaling. We next treated iCD103 cells with TiPARP inhibitor RBN2397
336 and observed expression of IL-6 was increased by ~2.5-fold when TiPARP was inhibited
337 indicating production of TiPARP by canonical AHR signaling significantly inhibits non-canonical
338 signaling and decreases production of inflammatory IL-6 (Fig. 4D). We next examined levels of
339 IL-6 in BLM treated WT or $AHR_{\Delta ex2}$ mice that had been treated with the complete AHR inhibitor
340 CH223191. In agreement with the increased IL-6 we observed in iCD103 DCs, $AHR_{\Delta ex2}$ mice
341 exhibited increased expression of IL-6 both in whole lung and in CD11c+ cells isolated by
342 magnetic bead purification from single cell lung digestions (Fig. 4E and 4F). Expression of IL-6
343 could be diminished by AHR inhibition (CCH223191) both at the whole lung and CD11c+ cell
344 level indicating a direct effect of AHR in CD11c+ cells in potentiating IL-6 production in the
345 fibrotic lung (Fig. 4E and 4F). Furthermore, we verified that expression of TiPARP was similarly
346 down-regulated in lung CD11c+ cells from $AHR_{\Delta ex2}$ mice and thus conclude that the increased
347 IL-6 observed is a product of the loss of anti-inflammatory canonical AHR signaling and a
348 concomitant increase in pro-inflammatory non-canonical AHR signaling.

349 **DC ncAHR signaling potentiates IL-17 production from lymphocytes.** Given that $AHR_{\Delta ex2}$
350 mice developed increased fibrosis and that ex-vivo generated DCs produced increased IL-6 in
351 response to TLR9 stimulus, we next examined if $AHR_{\Delta ex2}$ mice would over-produce IL-17 in
352 response to BLM. We generated lung single cell suspensions at 7-days post-BLM and analyzed
353 expression of IL-17 in lymphocyte populations via flow cytometry. Flow cytometric analysis
354 revealed $AHR_{\Delta ex2}$ mice displayed increases in multiple IL-17 producing lymphocyte populations
355 including conventional Th17 cells, IL-17A producing gamma-delta T-cells, and putative IL-17A+
356 iNKT cells and ILC3s (Fig 5A quantified in 5B). Although we determined CD4+ lymphocytes
357 were not responsible for increased fibrosis (Fig. 4A), we noted the largest increase in IL-17A
358 expressing lymphocytes was in CD4- γδ TCR+ populations which would not be affected by CD4
359 depletion. $AHR_{\Delta ex2}$ mice expressed ~5-fold more IL-17 at 21-days post-BLM (Fig. 5C).
360 Production of both IL-6 and IL-17 was susceptible to complete inhibition of AHR via
361 administration of CH223191 (Fig. 4E, 4F and Supplemental Fig. 2) indicating DCs and
362 macrophages in CD11c-Cre / $AHR_{\Delta ex2}$ mice still had functional ncAHR signaling. We further
363 verified the involvement of CD103+ DCs by examining expression of IL-17 in the lungs of BLM

364 treated BATF3$^{-/-}$ mice and found that loss of CD103+ DCs almost completely abrogated lung IL-
365 17 responses (Fig. 5D).

366 **Fibroblasts from fibrotic lungs express kynurenine producing enzymes in response to**
367 **TLR9 stimulus.** Endogenous AHR ligands are largely produced as a result of the metabolism of
368 tryptophan along the kynurenine pathway by enzymes such as IDO1 and TDO2. To determine
369 what cells produce these enzymes in fibrotic lungs, we investigated data from two previously
370 published single-cell RNAseq studies of IPF.(36, 37) Over 9000 stromal cells from 36 controls
371 and 44 lungs were collectively analyzed and reclassified based on the markers and
372 nomenclature described in Adams et al.(37) Though IDO1 was undetected, expression of TDO2
373 was observed upregulated specifically in IPF alveolar fibroblasts across both datasets (Fig. 6A
374 and Supplemental Fig. 3). In addition to myeloid cells, TLR9 activation in fibroblasts has also
375 been shown to be important in driving fibrosis.(29, 53) Thus, we next isolated fibroblasts from
376 mouse lungs on d-21 post-Saline or BLM and subsequently treated these cells with ODN2395 to
377 simulate an inflammatory / fibrotic environment *ex vivo*. Expression of both IDO1 and TDO2
378 increased in ODN2395-treated fibroblasts from BLM-treated mice but not in ODN2395-treated
379 control fibroblasts (Fig. 6B and 6C). AHR was also upregulated in the same conditions (Fig 6D);
380 however, TLR9 was upregulated with ODN2395 regardless of BLM treatment (Fig 6E). We
381 further assayed for expression of the main enzymes involved in the production of kynurenine,
382 i.e., IDO1 and TDO2, in whole lung following BLM treatment. Interestingly, expression of IDO1
383 was decreased at both 7- and 14-days post BLM (Fig. 7A); however, TDO2 expression was
384 significantly increased at both time points (Fig. 7B) thus it appears that TDO2 is preferentially
385 induced over IDO1 in pulmonary fibrosis *in vivo*. To address the importance of TDO2 during
386 fibrosis we next treated groups of mice with the specific TDO2 inhibitor 680C91. Strikingly,
387 inhibition of TDO2 significantly decreased both collagen deposition and expression of the
388 myofibroblast marker alpha smooth muscle actin (αSMA) during BLM induced pulmonary
389 fibrosis as well fibrotic pathology as assessed by trichrome staining of lung sections (Fig. 7C,
390 7D, and 7E).

391 **Discussion**

392 **Role of DCs in regulating pulmonary fibrosis.** The role of myeloid cells, especially DCs, in
393 altering immune responses during development / exacerbation of pulmonary fibrosis is currently
394 not well understood. Increased numbers of DC subsets infiltrate lungs of IPF patients and mice
395 with pulmonary fibrosis.(8, 54-56) However, the study of DCs in pulmonary fibrosis has been
396 overlooked due to publication of seminal work demonstrating that CD4+ and CD8+

397 lymphocytes, and by extension the DCs that prime those responses, are not important in
398 mediating fibrotic effects.(57) Recently, it is appreciated that DCs can modulate immune
399 responses outside of antigen presentation through production of pro-inflammatory / fibrotic
400 cytokines. We, and others, have demonstrated that lung DCs can prime and activate pathogenic
401 IL-17 responses through production of inflammatory cytokines such as IL-6 and TGF-β in innate
402 lymphocytes as well as CD4+ T cells.(5, 58)

403 Here we demonstrate CD103+ DCs infiltrate the fibrotic lung and mediate production of
404 pro-inflammatory / fibrotic cytokines through cooperation of AHR and pro-inflammatory TLR
405 signaling. We noted significant accumulation of CD103+ DCs in lungs of BLM-treated mice
406 beginning in the early inflammatory phase (7-days post-treatment) and continuing into the
407 fibrotic phase (21-days post treatment, Fig. 1F). Loss of CD103+ DCs in BATF3$^{-/-}$ mice was
408 protective indicating a pathogenic role for lung resident DCs (Fig. 1B – 1E). In agreement with
409 our previously published study(4), CD103 cells that infiltrate the fibrotic lung express high levels
410 of AHR (Fig. 1F). Canonical AHR signaling is immuno-suppressive and AHR target genes such
411 as TiPARP can constrain production of interferons and pro-inflammatory cytokines via ADP-
412 ribosylation of activators of NF-κB signaling such as TBK1.(44-47) Alternatively, ncAHR
413 signaling is well characterized to bind NF-κB subunits like RelA and RelB and enhance
414 production of pro-inflammatory cytokines.(27, 48-50) We noted increased expression of IL-6
415 following BLM both in the whole lung and from isolated CD11c+ cells which correlated with
416 increased expression of AHR (Fig. 1); however, expression of the AHR inducible gene product,
417 Cyp1b1 was significantly decreased (Fig. 1H). Thus, even though CD11c+ cells express AHR
418 and there is abundant AHR ligand produced in fibrotic lungs (Fig. 2A), these cells do not
419 activate canonical AHR signaling and instead activate pro-inflammatory ncAHR signaling in the
420 BLM treated lungs.

421 **Role of ncAHR / NF-Kb and TIPARP in modulating cellular cytokine responses.** The role of
422 tryptophan metabolism and AHR signaling in mediating pulmonary fibrosis is unclear.
423 Kynurenine / tryptophan ratios increase in serum and lungs of patients with interstitial
424 pneumonia and treatment with anti-fibrotic Pirfenidone significantly decreased levels of
425 kynurenine suggesting a positive correlation between tryptophan metabolism, AHR activation,
426 and development of fibrosis.(12, 59) More recently, activation of AHR through exogenous
427 administration of AHR ligand FICZ ameliorated pulmonary fibrosis presumably by augmenting
428 numbers of FoxP3+ regulatory T-cells, and decreasing IFNγ+ CD4+ T-cells and IL-17A+ γδ+ T-
429 cells.(60) However, this study did not look specifically at AHR signaling in pulmonary immune

430 cells nor did it demonstrate if FICZ is produced during fibrosis. Furthermore, mice were treated
431 directly after administration of BLM on days 0, 1, and 2 making it difficult to determine direct
432 effects of pulmonary AHR signaling in inhibiting fibrosis versus modulating early lung injury post-
433 BLM. We detected significantly elevated kynurenine from 7 – 14 days post-BLM corresponding
434 to the early fibrotic phase of BLM induced fibrosis (Fig. 2A). In contrast to previous work,
435 complete inhibition of AHR signaling via administration of CH223191 reduced fibrosis when
436 started late in the progression of disease (10-days post-BLM) indicating a role for pulmonary
437 AHR signaling in promoting fibrogenesis (Fig. 2B – 2C).

438 We generated mice that lacked canonical AHR signaling in CD11c+ cells including
439 pulmonary DCs and macrophage (Fig. 3A and Supplemental Fig. 1). Interestingly, while DCs
440 produced from these mice lacked canonical AHR signaling (Fig. 3B), we still detected AHR at
441 the transcript and protein level (Fig. 3C – 4E). Furthermore, sequencing cDNA generated from
442 $AHR_{\Delta ex2}$ DCs indicated an alternative start codon is formed when exon 2 is deleted
443 (Supplemental Fig. 1A). Together, these data indicated that a truncated AHR product still
444 mediated ncAHR interactions. When we administered BLM to $AHR_{\Delta ex2}$ mice we noted more
445 fibrosis that was still AHR-dependent (Fig. 3F and 3G) indicating loss of canonical AHR
446 signaling in CD11c+ cells resulted in increased ncAHR signaling that exacerbated pulmonary
447 fibrosis.

448 To determine if increased fibrosis seen in $AHR_{\Delta ex2}$ was intrinsic to DCs we adoptively
449 transferred ex-vivo generated iCD103 DCs from $AHR_{\Delta ex2}$ mice into BLM treated B6 mice and
450 noted more fibrosis when DCs from CD11c-Cre+ / $AHR_{\Delta ex2}$ were transferred in comparison to
451 either Cre- cells (data not shown) or non-transferred mice (Fig. 4A). We further show AHR can
452 synergize with TLR9 activation and promote expression of IL-6 in DCs; however, expression of
453 canonical AHR genes that limit cytokine production, e.g., TiPARP is lost in $AHR_{\Delta ex2}$ DCs (Fig 4B
454 – 4D). Thus, BLM-induced fibrosis results in increased expression of AHR; however, the
455 signaling is shunted towards non-canonical signaling resulting in increased expression of pro-
456 inflammatory cytokines. It is currently unclear why ncAHR signaling is promoted over canonical
457 signaling in fibrotic lungs, however, several transcription factors such as HIF1α which are up-
458 regulated during fibrogenesis bind to the canonical AHR partner ARNT (HIF1β).(61) Thus, it is
459 plausible that dimerization of HIF1α-ARNT may reduce the available pool of ARNT which
460 promotes AHR-NFκB dimerization shifting the balance of AHR signaling from canonical, anti-
461 inflammatory, to non-canonical, inflammatory, signaling which drives excessive fibrogenesis.

462 **Role of IL-6 in promoting profibrotic IL-17 responses.** The role of the IL-6 – IL-17 axis is
463 appreciated in the progression of pulmonary fibrosis. Depletion of either IL-6 or IL-17 is
464 protective for BLM-induced fibrosis and we have previously published that IL-17 can act directly
465 on fibroblasts to promote collagen production and fibroproliferation.(5, 62-64) Even in IPF
466 patients, expression of IL-6 and IL-17 isoforms are associated with more rapid time to death or
467 lung transplantation (Supplemental Fig. 3).

468 In agreement with this we isolated fibroblasts from control or BLM-treated mice and
469 treated with the TLR9 agonist, ODN2395. TLR9 activation upregulated expression of both IDO1
470 and TDO2 in BLM fibroblasts but not control (WT) fibroblasts, we corroborated expression of
471 TDO2 in IPF patient myofibroblasts, however, we did not detect appreciable expression of IDO1
472 in human myofibroblasts and overall expression of IDO1 was shown to decrease in the lungs of
473 fibrotic mice while expression of TDO2 increased (Fig. 6A – 6C, 7A and7B). Treatment of mice
474 with the TDO2 inhibitor 680C91 ameliorated fibrosis, reducing collagen production, and
475 decreasing expression of the myofibroblast marker αSMA (Fig. 7C, 7D, and 7E). Furthermore,
476 we noted increased expression of AHR and TLR9 itself following TLR9 stimulation in BLM
477 fibroblasts indicating that AHR plays a fundamentally pro-fibrotic role (Fig. 6D – 6E). However,
478 In direct contrast to this, a previous study found that treatment of fibroblasts with the AHR
479 activating compound ITE inhibited TGFβ induced myofibroblast differentiation and collagen
480 production.(28) The exact cause for the discrepancy between these two studies will require
481 further investigation, however, it is plausible that induction of AHR signaling in the context of
482 inflammatory stimulus, e.g., TLR stimulation as would happen in the fibrotic lung behaves
483 fundamentally different than in an isolated *ex vivo* condition. Expression of TLR9 is associated
484 with rapid progression of IPF in patients and loss of TLR9 signaling is protective from BLM-
485 induced fibrosis.(29, 51, 52) Furthermore, fibroblasts isolated from IPF patients that had more
486 robust activation profiles when exposed to TLR9 agonist correlated with increased AHR
487 activation in matched myeloid cells.(30)

488 Together, these studies indicate that a fibrogenic circuit is established between TLR9+
489 fibroblasts and AHR+ myeloid cells that is important in progression of pulmonary fibrosis
490 through modulation of pro-fibrotic cytokines like IL-6 and IL-17 (Working model in Fig. 8). More
491 work is needed to fully understand the switch to ncAHR signaling during fibrogenesis and to
492 understand the spatial crosstalk between fibroblasts and DCs. However, given the need for new
493 treatments for IPF patients, drugs that modulate kynurenine pathway enzymes, i.e., IDO1 and
494 TDO2, or AHR directly represent an exciting possibility with untapped therapeutic potential.

495 **References**

496 1. Raghu G, Collard HR, Egan JJ, Martinez FJ, Behr J, Brown KK, et al. An official ATS/ERS/JRS/ALAT
497 statement: idiopathic pulmonary fibrosis: evidence-based guidelines for diagnosis and
498 management. *Am J Respir Crit Care Med.* 2011;183(6):788-824.
499 2. Chambers DC, Cherikh WS, Harhay MO, Hayes D, Hsich E, Khush KK, et al. The International
500 Thoracic Organ Transplant Registry of the International Society for Heart and Lung
501 Transplantation: Thirty-sixth adult lung and heart-lung transplantation Report-2019; Focus
502 theme: Donor and recipient size match. *J Heart Lung Transplant.* 2019;38(10):1042-55.
503 3. Douglas WW, Ryu JH, and Schroeder DR. Idiopathic pulmonary fibrosis: Impact of oxygen and
504 colchicine, prednisone, or no therapy on survival. *Am J Respir Crit Care Med.* 2000;161(4 Pt
505 1):1172-8.
506 4. Gurczynski SJ, Pereira NL, Hrycaj SM, Wilke C, Zemans RL, and Moore BB. Stem cell
507 transplantation uncovers TDO-AHR regulation of lung dendritic cells in herpesvirus-induced
508 pathology. *JCI Insight.* 2021;6(2).
509 5. Zhou X, Loomis-King H, Gurczynski SJ, Wilke CA, Konopka KE, Ptaschinski C, et al. Bone marrow
510 transplantation alters lung antigen-presenting cells to promote TH17 response and the
511 development of pneumonitis and fibrosis following gammaherpesvirus infection. *Mucosal*
512 *Immunol.* 2016;9(3):610-20.
513 6. Misharin AV, Morales-Nebreda L, Mutlu GM, Budinger GR, and Perlman H. Flow cytometric
514 analysis of macrophages and dendritic cell subsets in the mouse lung. *Am J Respir Cell Mol Biol.*
515 2013;49(4):503-10.
516 7. Marchal-Somme J, Uzunhan Y, Marchand-Adam S, Kambouchner M, Valeyre D, Crestani B, et al.
517 Dendritic cells accumulate in human fibrotic interstitial lung disease. *Am J Respir Crit Care Med.*
518 2007;176(10):1007-14.
519 8. Tsoumakidou M, Karagiannis KP, Bouloukaki I, Zakynthinos S, Tzanakis N, and Siafakas NM.
520 Increased bronchoalveolar lavage fluid CD1c expressing dendritic cells in idiopathic pulmonary
521 fibrosis. *Respiration; international review of thoracic diseases.* 2009;78(4):446-52.
522 9. Piwarski SA, and Salisbury TB. The effects of environmental aryl hydrocarbon receptor ligands on
523 signaling and cell metabolism in cancer. *Biochem Pharmacol.* 2023;216:115771.
524 10. Poland A, Glover E, and Kende AS. Stereospecific, high affinity binding of 2,3,7,8-
525 tetrachlorodibenzo-p-dioxin by hepatic cytosol. Evidence that the binding species is receptor for
526 induction of aryl hydrocarbon hydroxylase. *J Biol Chem.* 1976;251(16):4936-46.
527 11. Adams S, Braidy N, Bessede A, Brew BJ, Grant R, Teo C, et al. The kynurenine pathway in brain
528 tumor pathogenesis. *Cancer Res.* 2012;72(22):5649-57.
529 12. Meyer KC, Arend RA, Kalayoglu MV, Rosenthal NS, Byrne GI, and Brown RR. Tryptophan
530 metabolism in chronic inflammatory lung disease. *J Lab Clin Med.* 1995;126(6):530-40.
531 13. Mandarano M, Orecchini E, Bellezza G, Vannucci J, Ludovini V, Baglivo S, et al.
532 Kynurenine/Tryptophan Ratio as a Potential Blood-Based Biomarker in Non-Small Cell Lung
533 Cancer. *Int J Mol Sci.* 2021;22(9).
534 14. Wang M, Dong X, Huang Y, Su J, Dai X, Guo Y, et al. Activation of the kynurenine pathway is
535 associated with poor outcome in Pneumocystis pneumonia patients infected with HIV: results of
536 2 months cohort study. *BMC Infect Dis.* 2019;19(1):223.
537 15. Zinellu A, Fois AG, Zinellu E, Sotgiu E, Sotgia S, Arru D, et al. Increased kynurenine plasma
538 concentrations and kynurenine-tryptophan ratio in mild-to-moderate chronic obstructive
539 pulmonary disease patients. *Biomark Med.* 2018;12(3):229-37.

16. Almulla AF, Supasitthumrong T, Tunvirachaisakul C, Algon AAA, Al-Hakeim HK, and Maes M. The tryptophan catabolite or kynurenine pathway in COVID-19 and critical COVID-19: a systematic review and meta-analysis. *BMC Infect Dis.* 2022;22(1):615.
17. Cihan M, Doğan Ö, Ceran Serdar C, Altunçekiç Yıldırım A, Kurt C, and Serdar MA. Kynurenine pathway in Coronavirus disease (COVID-19): Potential role in prognosis. *J Clin Lab Anal.* 2022;36(3):e24257.
18. D'Amora P, Silva IDCG, Budib MA, Ayache R, Silva RMS, Silva FC, et al. Towards risk stratification and prediction of disease severity and mortality in COVID-19: Next generation metabolomics for the measurement of host response to COVID-19 infection. *PLoS One.* 2021;16(12):e0259909.
19. Henry EC, and Gasiewicz TA. Transformation of the aryl hydrocarbon receptor to a DNA-binding form is accompanied by release of the 90 kDa heat-shock protein and increased affinity for 2,3,7,8-tetrachlorodibenzo-p-dioxin. *Biochem J.* 1993;294 (Pt 1)(Pt 1):95-101.
20. Whitelaw M, Pongratz I, Wilhelmsson A, Gustafsson JA, and Poellinger L. Ligand-dependent recruitment of the Arnt coregulator determines DNA recognition by the dioxin receptor. *Mol Cell Biol.* 1993;13(4):2504-14.
21. Wang GL, Jiang BH, Rue EA, and Semenza GL. Hypoxia-inducible factor 1 is a basic-helix-loop-helix-PAS heterodimer regulated by cellular O2 tension. *Proc Natl Acad Sci U S A.* 1995;92(12):5510-4.
22. Okino ST, Pendurthi UR, and Tukey RH. Phorbol esters inhibit the dioxin receptor-mediated transcriptional activation of the mouse Cyp1a-1 and Cyp1a-2 genes by 2,3,7,8-tetrachlorodibenzo-p-dioxin. *J Biol Chem.* 1992;267(10):6991-8.
23. Wright EJ, De Castro KP, Joshi AD, and Elferink CJ. Canonical and non-canonical aryl hydrocarbon receptor signaling pathways. *Curr Opin Toxicol.* 2017;2:87-92.
24. Wilson SR, Joshi AD, and Elferink CJ. The tumor suppressor Kruppel-like factor 6 is a novel aryl hydrocarbon receptor DNA binding partner. *J Pharmacol Exp Ther.* 2013;345(3):419-29.
25. Ho CC, Lee HL, Chen CY, Luo YH, Tsai MH, Tsai HT, et al. Involvement of the cytokine-IDO1-AhR loop in zinc oxide nanoparticle-induced acute pulmonary inflammation. *Nanotoxicology.* 2017;11(3):360-70.
26. Vogel CF, Khan EM, Leung PS, Gershwin ME, Chang WL, Wu D, et al. Cross-talk between aryl hydrocarbon receptor and the inflammatory response: a role for nuclear factor-κB. *J Biol Chem.* 2014;289(3):1866-75.
27. Kado S, Chang WLW, Chi AN, Wolny M, Shepherd DM, and Vogel CFA. Aryl hydrocarbon receptor signaling modifies Toll-like receptor-regulated responses in human dendritic cells. *Arch Toxicol.* 2017;91(5):2209-21.
28. Lehmann GM, Xi X, Kulkarni AA, Olsen KC, Pollock SJ, Baglole CJ, et al. The aryl hydrocarbon receptor ligand ITE inhibits TGFbeta1-induced human myofibroblast differentiation. *Am J Pathol.* 2011;178(4):1556-67.
29. Trujillo G, Meneghin A, Flaherty KR, Sholl LM, Myers JL, Kazerooni EA, et al. TLR9 differentiates rapidly from slowly progressing forms of idiopathic pulmonary fibrosis. *Science translational medicine.* 2010;2(57):57ra82.
30. Huang Y, Ma SF, Espindola MS, Vij R, Oldham JM, Huffnagle GB, et al. Microbes Are Associated with Host Innate Immune Response in Idiopathic Pulmonary Fibrosis. *Am J Respir Crit Care Med.* 2017;196(2):208-19.
31. Wang F, Liu M, Ma D, Cai Z, Liu L, Wang J, et al. Dendritic cell-expressed IDO alleviates atherosclerosis by expanding CD4. *Int Immunopharmacol.* 2023;116:109758.
32. Rankin LC, Kaiser KA, de Los Santos-Alexis K, Park H, Uhlemann AC, Gray DHD, et al. Dietary tryptophan deficiency promotes gut RORγt. *Cell Rep.* 2023;42(3):112135.

587 33. Holloman BL, Cannon A, Wilson K, Nagarkatti P, and Nagarkatti M. Aryl Hydrocarbon Receptor
588 Activation Ameliorates Acute Respiratory Distress Syndrome through Regulation of Th17 and
589 Th22 Cells in the Lungs. *mBio.* 2023:e0313722.
590 34. Mayer CT, Ghorbani P, Nandan A, Dudek M, Arnold-Schrauf C, Hesse C, et al. Selective and
591 efficient generation of functional Batf3-dependent CD103+ dendritic cells from mouse bone
592 marrow. *Blood.* 2014;124(20):3081-91.
593 35. Woroniecka KI, Rhodin KE, Dechant C, Cui X, Chongsathidkiet P, Wilkinson D, et al. 4-1BB
594 Agonism Averts TIL Exhaustion and Licenses PD-1 Blockade in Glioblastoma and Other
595 Intracranial Cancers. *Clin Cancer Res.* 2020;26(6):1349-58.
596 36. Habermann AC, Gutierrez AJ, Bui LT, Yahn SL, Winters NI, Calvi CL, et al. Single-cell RNA
597 sequencing reveals profibrotic roles of distinct epithelial and mesenchymal lineages in
598 pulmonary fibrosis. *Sci Adv.* 2020;6(28):eaba1972.
599 37. Adams TS, Schupp JC, Poli S, Ayaub EA, Neumark N, Ahangari F, et al. Single-cell RNA-seq reveals
600 ectopic and aberrant lung-resident cell populations in idiopathic pulmonary fibrosis. *Sci Adv.*
601 2020;6(28):eaba1983.
602 38. Gurczynski SJ, Procario MC, O'Dwyer DN, Wilke CA, and Moore BB. Loss of CCR2 signaling alters
603 leukocyte recruitment and exacerbates gamma-herpesvirus-induced pneumonitis and fibrosis
604 following bone marrow transplantation. *Am J Physiol Lung Cell Mol Physiol.* 2016;311(3):L611-
605 27.
606 39. Gurczynski SJ, Zhou X, Flaherty M, Wilke CA, and Moore BB. Bone marrow transplant-induced
607 alterations in Notch signaling promote pathologic Th17 responses to gamma-herpesvirus
608 infection. *Mucosal Immunol.* 2018;11(3):881-93.
609 40. Bowman WS, Newton CA, Linderholm AL, Neely ML, Pugashetti JV, Kaul B, et al. Proteomic
610 biomarkers of progressive fibrosing interstitial lung disease: a multicentre cohort analysis.
611 *Lancet Respir Med.* 2022;10(6):593-602.
612 41. Hildner K, Edelson BT, Purtha WE, Diamond M, Matsushita H, Kohyama M, et al. Batf3 deficiency
613 reveals a critical role for CD8alpha+ dendritic cells in cytotoxic T cell immunity. *Science.*
614 2008;322(5904):1097-100.
615 42. Badawy AA. Kynurenine Pathway of Tryptophan Metabolism: Regulatory and Functional
616 Aspects. *Int J Tryptophan Res.* 2017;10:1178646917691938.
617 43. Walisser JA, Glover E, Pande K, Liss AL, and Bradfield CA. Aryl hydrocarbon receptor-dependent
618 liver development and hepatotoxicity are mediated by different cell types. *Proc Natl Acad Sci U S*
619 *A.* 2005;102(49):17858-63.
620 44. Matthews J. AHR toxicity and signaling: Role of TIPARP and ADP-ribosylation. *Current Opinion in*
621 *Toxicology.* 2017;2:50-7.
622 45. Yamada T, Horimoto H, Kameyama T, Hayakawa S, Yamato H, Dazai M, et al. Constitutive aryl
623 hydrocarbon receptor signaling constrains type I interferon-mediated antiviral innate defense.
624 *Nat Immunol.* 2016;17(6):687-94.
625 46. Kozaki T, Komano J, Kanbayashi D, Takahama M, Misawa T, Satoh T, et al. Mitochondrial damage
626 elicits a TCDD-inducible poly(ADP-ribose) polymerase-mediated antiviral response. *Proc Natl*
627 *Acad Sci U S A.* 2017;114(10):2681-6.
628 47. Ahmed S, Bott D, Gomez A, Tamblyn L, Rasheed A, Cho T, et al. Loss of the Mono-ADP-
629 ribosyltransferase, Tiparp, Increases Sensitivity to Dioxin-induced Steatohepatitis and Lethality. *J*
630 *Biol Chem.* 2015;290(27):16824-40.
631 48. Chen PH, Chang H, Chang JT, and Lin P. Aryl hydrocarbon receptor in association with RelA
632 modulates IL-6 expression in non-smoking lung cancer. *Oncogene.* 2012;31(20):2555-65.
633 49. Vogel CF, Sciullo E, Li W, Wong P, Lazennec G, and Matsumura F. RelB, a new partner of aryl
634 hydrocarbon receptor-mediated transcription. *Mol Endocrinol.* 2007;21(12):2941-55.

50. Vogel CF, Wu D, Goth SR, Baek J, Lollies A, Domhardt R, et al. Aryl hydrocarbon receptor signaling regulates NF-kappaB RelB activation during dendritic-cell differentiation. *Immunol Cell Biol.* 2013;91(9):568-75.
51. Hogaboam CM, Trujillo G, and Martinez FJ. Aberrant innate immune sensing leads to the rapid progression of idiopathic pulmonary fibrosis. *Fibrogenesis Tissue Repair.* 2012;5(Suppl 1):S3.
52. Alzahrani B, Gaballa MMS, Tantawy AA, Moussa MA, Shoulah SA, and Elshafae SM. Blocking Toll-like receptor 9 attenuates bleomycin-induced pulmonary injury. *J Pathol Transl Med.* 2022;56(2):81-91.
53. Fang F, Marangoni RG, Zhou X, Yang Y, Ye B, Shangguang A, et al. Toll-like Receptor 9 Signaling Is Augmented in Systemic Sclerosis and Elicits Transforming Growth Factor beta-Dependent Fibroblast Activation. *Arthritis Rheumatol.* 2016;68(8):1989-2002.
54. Chakraborty K, Chatterjee S, and Bhattacharyya A. Modulation of CD11c+ lung dendritic cells in respect to TGF-beta in experimental pulmonary fibrosis. *Cell biology international.* 2017;41(9):991-1000.
55. Serezani APM, Pascoalino BD, Bazzano JMR, Vowell KN, Tanjore H, Taylor CJ, et al. Multiplatform Single-Cell Analysis Identifies Immune Cell Types Enhanced in Pulmonary Fibrosis. *Am J Respir Cell Mol Biol.* 2022;67(1):50-60.
56. Bantsimba-Malanda C, Marchal-Somme J, Goven D, Freynet O, Michel L, Crestani B, et al. A role for dendritic cells in bleomycin-induced pulmonary fibrosis in mice? *Am J Respir Crit Care Med.* 2010;182(3):385-95.
57. Helene M, Lake-Bullock V, Zhu J, Hao H, Cohen DA, and Kaplan AM. T cell independence of bleomycin-induced pulmonary fibrosis. *J Leukoc Biol.* 1999;65(2):187-95.
58. Wilke CA, Chadwick MM, Chan PR, Moore BB, and Zhou X. Stem cell transplantation impairs dendritic cell trafficking and herpesvirus immunity. *JCI Insight.* 2019;4(18).
59. Fois AG, Sotgiu E, Scano V, Negri S, Mellino S, Zinellu E, et al. Effects of Pirfenidone and Nintedanib on Markers of Systemic Oxidative Stress and Inflammation in Patients with Idiopathic Pulmonary Fibrosis: A Preliminary Report. *Antioxidants (Basel).* 2020;9(11).
60. Takei H, Yasuoka H, Yoshimoto K, and Takeuchi T. Aryl hydrocarbon receptor signals attenuate lung fibrosis in the bleomycin-induced mouse model for pulmonary fibrosis through increase of regulatory T cells. *Arthritis Res Ther.* 2020;22(1):20.
61. Epstein Shochet G, Bardenstein-Wald B, McElroy M, Kukuy A, Surber M, Edelstein E, et al. Hypoxia Inducible Factor 1A Supports a Pro-Fibrotic Phenotype Loop in Idiopathic Pulmonary Fibrosis. *Int J Mol Sci.* 2021;22(7).
62. Wilson MS, Madala SK, Ramalingam TR, Gochuico BR, Rosas IO, Cheever AW, et al. Bleomycin and IL-1beta-mediated pulmonary fibrosis is IL-17A dependent. *J Exp Med.* 2010;207(3):535-52.
63. Cipolla E, Fisher AJ, Gu H, Mickler EA, Agarwal M, Wilke CA, et al. IL-17A deficiency mitigates bleomycin-induced complement activation during lung fibrosis. *FASEB journal : official publication of the Federation of American Societies for Experimental Biology.* 2017;31(12):5543-56.
64. Saito F, Tasaka S, Inoue K, Miyamoto K, Nakano Y, Ogawa Y, et al. Role of interleukin-6 in bleomycin-induced lung inflammatory changes in mice. *Am J Respir Cell Mol Biol.* 2008;38(5):566-71.

Figure Legends

Figure 1. CD103+ DCs accumulate in the fibrotic lung and show evidence of pro-inflammatory AHR signaling. A and B) Mice (n = 6 – 10 mice per group (panel A), 5 per group (panel B) were treated with 0 75 U/kg bleomycin for 0, 7 or 14 days (panel A) or 14 days (panel B). Lungs were harvested and single cell suspensions were analyzed by flow cytometry for the presence of CD103+ DCs (CD45+, CD11c+, MHCII+, CD24+, CD64-, CD103+). **(C, D, and E)** groups of mice (n = 5-8 mice per group (panel C) or n = 6-8 per group (panel D and E)) were treated with 0.75 U/kg BLM for 14 – 21 days. Lungs were harvested and collagen was quantified by hydroxyproline assay or qRT-PCR. **F)** Mice (n = 4 per group) were treated with 0.75 U/kg BLM for 7 days after which lungs were harvested and single cell suspensions were analyzed via flow cytometry for AHR expression in the indicated cell subsets. **G through I)** Mice (n = 5 per group) were treated with 0.75 U/kg bleomycin or saline control (WT). Single cell suspensions were prepared from collagenase digested lung tissue at 7-days post bleomycin and CD11c+ cells were purified via magnetic bead isolation. Expression of the indicated transcripts was analyzed via qRT-PCR. All experiments shown are representative of at least three independent experiments, statistical significance was determined via ANOVA in panel A and C-E, or student's t-test in panels G-I (* = $p < 0.05$, ** = $p < 0.01$, *** = $p < 0.001$, **** = $p < 0.0001$).

Figure 2. Production of AHR ligands is augmented during BLM induced fibrosis and complete AHR inhibition ameliorates disease. A) Mice (n = 4-5 mice per group) were treated with 0.75 U/kg BLM. Lungs were harvested at the indicated times and whole lung homogenates were assayed for KYN concentration by ELISA. **B)** Mice, (n = 3 – 5 per group) were treated with 0.75 U/kg bleomycin. Beginning at day 10 mice were treated daily with 5 mg/kg CH223191 dissolved in a vehicle of 2% Tween-20, 0.5% Carboxy methylcellulose, in PBS or vehicle alone by oral gavage until day 18. Lungs were harvested at Day 21 and lung collagen was quantified by hydroxyproline assay. **C)** Representative histology of lungs from B). Sections were stained with trichrome which highlights collagen fibers as blue staining (scale bar = 50 μM). All experiments shown are representative of at least three independent experiments, statistical significance was determined via ANOVA (* = $p < 0.05$, ** = $p < 0.01$, **** = $p < 0.0001$).

Figure 3. Deletion of AHR exon-2 reduces canonical AHR signaling in DCs but AHR expression is retained and augments inflammatory non-canonical AHR signaling. A) Cartoon schematic of murine AHR depicting the deletion of AHR exon-2 containing the DNA binding bHLH domain. Numbered boxes correlate to individual exons. **(B and C)** iCD103+ DCs were generated from WT B6 mice or $AHR_{\Delta ex2}$ mice and treated with 200 μM KYN or 10 μM CH223191 (CH223). 18 hours after treatment, RNA was harvested and expression of the canonical AHR gene Cyp1b1 (A) or AHR (B) was analyzed via qRT-PCR. **D)** iCD103+ DCs were analyzed via flow cytometry for expression of CD11c and CD103 as well as intracellular expression of AHR. **E)** Representative histogram showing AHR expression in WT or $AHR_{\Delta ex2}$ iCD103 DCs analyzed via flow cytometry. **F and G)** Mice (n = 5 per group) were treated with 0.75 U/kg bleomycin. At 10-d post bleomycin groups of mice were administered CH223191 (5 mg/kg) or vehicle alone daily until 18-d post bleomycin. Lungs were harvested at 21-d post bleomycin collagen content was quantified via hydroxyproline assay (F) and lung fibrosis was examined via histopathologic examination of fixed lung sections (A: Scale bar = 100 μM panel G). All experiments shown are representative of at least three independent experiments, statistical significance was determined via ANOVA in panel A or student's t-test in panel B (* = $p < 0.05$, ** = $p < 0.01$, **** = $p < 0.0001$).

Figure 4. Loss of canonical AHR signaling in CD11c+ cells exacerbates fibrosis via a ncAHR dependent mechanism. A) Mice (n = 7 mice no transfer group and 11 mice Cre+ transfer groups) were treated with 0.75 U/kg bleomycin. At 1-d post-BLM $1x10^6$ iCD103 cells

732 generated from naïve CD11c-Cre+ $AHR_{\Delta ex2}$ mice were adoptively transferred via tail vein
733 injection. Additionally, one group was administered 100 µg αCD4 neutralizing antibody at 1-
734 and 7-d post bleomycin. Lungs were harvested 21-d post bleomycin and collagen content was
735 quantified via hydroxyproline assay. **B through D)** iCD103 cells were generated as described.
736 Cells were stimulated with 1 µM ODN2395 (TLR9 agonist), 10 µM RBN2397 (TiPARP inhibitor),
737 or a vehicle control for 18 hours. Cells were harvested and RNA was analyzed for expression of
738 IL-6 or TiPARP transcript via qRT-PCR. **E)** WT-B6 or $AHR_{\Delta ex2}$ mice were treated with 0.75 U/kg
739 BLM, CH223191 (CH223) was administered from day 10- to 18-post BLM. Lungs were
740 harvested at 21-day post BLM and expression of IL-6 transcript were quantified via qRT-PCR. **F**
741 **and G)** Mice (n = 5 - 7 per group) were treated with 0.75 U/kg bleomycin or saline control (WT).
742 Single cell suspensions were prepared from collagenase digested lung tissue at 7-days post
743 bleomycin and CD11c+ cells were purified via magnetic bead isolation after which cells were
744 pooled and treated overnight *ex-vivo* (n = 4 per group*)* with either 30µM CH223191 (CH223) or
745 DMSO vehicle control. Expression of the indicated transcripts was analyzed via qRT-PCR. All
746 experiments shown are representative of at least three independent experiments, statistical
747 significance was determined via ANOVA (* = $p < 0.05$, ** = $p < 0.01$, *** = $p < 0.001$, **** = $p <$
748 0.0001).
749
750 **Figure 5. ncAHR signaling in CD11c+ cells drives IL-17 production in the lung. A)** WT B6
751 or $AHR_{\Delta ex2}$ mice (n = 5 per group) were treated o.p. with 0.75 U/kg BLM. 7-days post-BLM lungs
752 were harvested and lung leukocytes were analyzed by flow cytometry for the following
753 populations Th17 (CD45+, Thy1.2+, CD3+, CD4+, IL-17A+), IL-17+ γδ t-cell (CD45+, Thy1.2+,
754 CD3+, CD4-, γδ-TCR+, IL-17A+), IL-17+ ILC3 (CD45+, Thy1.2+, CD3-, CD4-, IL-17+), IL-17A+
755 iNKT (CD45+, Thy1.2+, CD4-, CD3+, γδ-TCR+, IL-17A+). **B)** Quantification of cell populations
756 identified in A. **C)** WT-B6 or $AHR_{\Delta ex2}$ mice were treated with 0.75 U/kg BLM, CH223191
757 (CH223) was administered from day 10- to 18-post BLM. Lungs were harvested at 21-day post
758 BLM and expression of IL-17 transcript was quantified via qRT-PCR. **D)** Mice (n = 5-8 per
759 group) were treated with 0.75 U/kg BLM. 21-days post BLM treatment, lungs were harvested
760 and expression of IL-17 transcript from whole lung was analyzed via qRT-PCR. All experiments
761 shown are representative of at least three independent experiments, statistical significance was
762 determined via ANOVA (* = $p < 0.05$, ** = $p < 0.01$, **** = $p < 0.0001$).
763
764 **Figure 6. Fibroblasts isolated from fibrotic individuals express the kynurenine pathway**
765 **enzymes IDO and TDO in response to TLR9 stimulation. A)** Uniform manifold approximation
766 and projections (UMAPs) of human lung stromal cells labeled by normalized expression of
767 TDO2, cell type, and disease. **B through E**) Lung fibroblasts were cultured from groups of mice
768 treated with BLM for 21-d or untreated as control. Fibroblasts were subsequently treated with
769 the TLR9 agonist ODN2395 (ODN) or vehicle control (veh) for 18-h. Expression of the indicated
770 transcript was analyzed via qRT-PCR. All experiments shown are representative of at least two
771 independent experiments, statistical significance was determined via ANOVA (* = $p < 0.05$, ** =
772 $p < 0.01$, *** = $p < 0.001$).
773
774 **Figure 7. Inhibition of TDO2 rescues BLM induced fibrosis. (A and B)** Groups of mice (n = 5
775 per group) were treated with 0.75 U/kg BLM or saline control for 7-14 days after which
776 expression of the indicated transcript was analyzed in whole lung via qRT-PCR. **(C and D)**
777 Group of mice (n = 8 – 9 per group) were treated with 0.75 U/kg BLM or saline control.
778 Beginning on day 10 one group was treated with 15 mg/kg TDO2 inhibitor (680C91) daily by
779 oral gavage until day 18 after which lungs were harvested and expression of the indicated
780 transcript was assayed via qRT-PCR. **(E)** Representative histology (n =2 mice per group)
781 showing assessment of collagen deposition by trichrome staining (blue staining) scale bar
782 represents 100µm. All experiments shown are representative of at least two independent

783 experiments, statistical significance was determined via ANOVA (* = $p < 0.05$, ** = $p < 0.01$, ***
784 = $p < 0.001$).
785
786 **Figure 8. Working model for how fibroblast DC crosstalk contributes to fibrosis.**
787 Myofibroblasts express the kynurenine pathway enzyme TDO2 in response to TLR9 stimulation.
788 Kynurenine pathway metabolites active ncAHR signaling in DCs which, in cooperation with
789 inflammatory TLR singling, augments production of IL-6 resulting in production of IL-17 from
790 lymphocytes. Fibroblasts can be directly activated by IL-17 resulting in collagen production and
791 fibroproliferation.
792
793
794
795

Figure 1

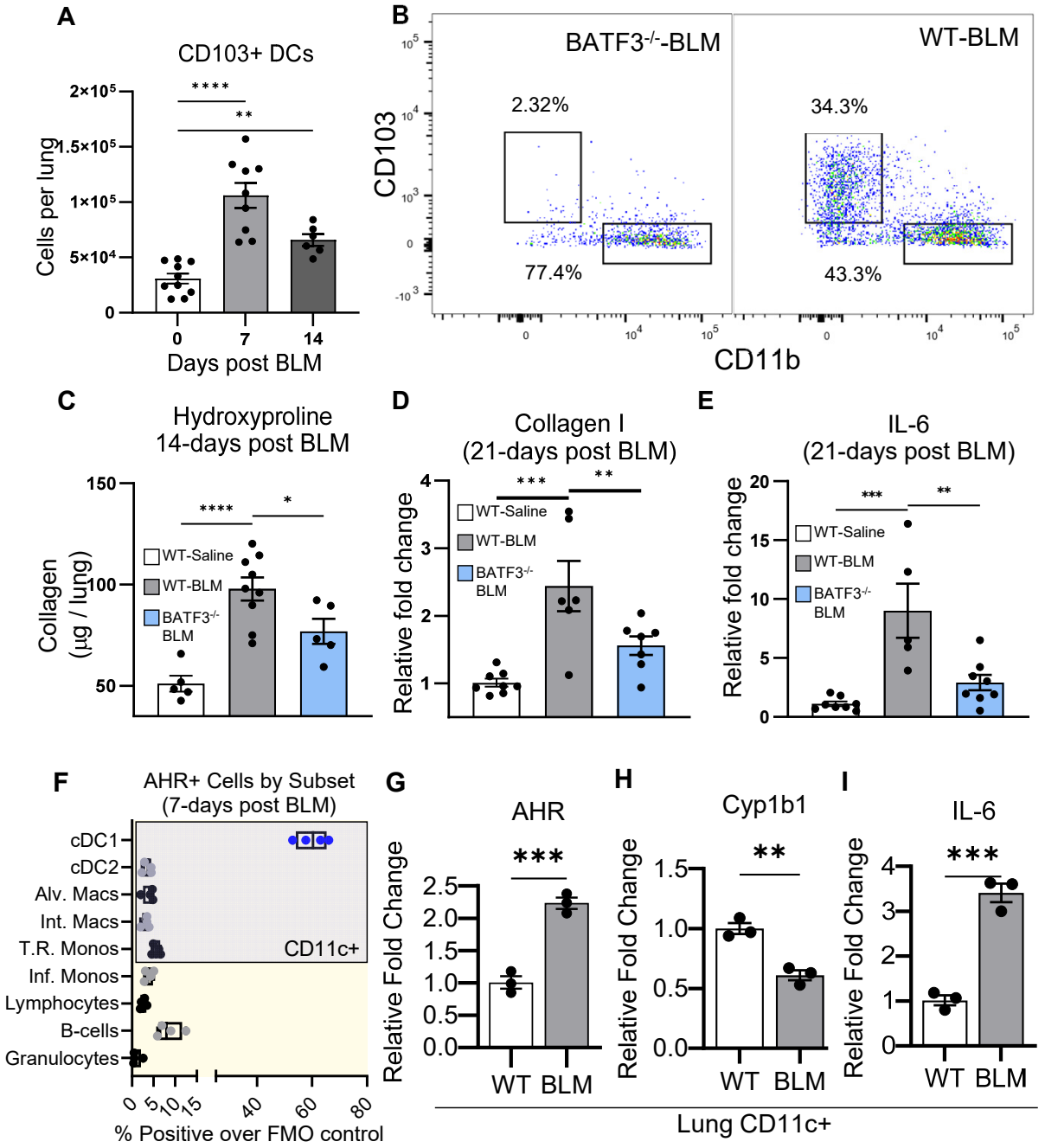

Figure 1. CD103+ DCs accumulate in the fibrotic lung and show evidence of pro-inflammatory AHR signaling. A and B) Mice (n = 6 – 10 mice per group (panel A), 5 per group (panel B) were treated with 0.75 U/kg bleomycin for 0, 7 or 14 days (panel A) or 14 days (panel B). Lungs were harvested and single cell suspensions were analyzed by flow cytometry for the presence of CD103+ DCs (CD45+, CD11c+, MHCII+, CD24+, CD64-, CD103+). **(C, D, and E)** groups of mice (n = 5-8 mice per group (panel C) or n = 6-8 per group (panel D and E)) were treated with 0.75 U/kg BLM for 14 – 21 days. Lungs were harvested and collagen was quantified by hydroxyproline assay or qRT-PCR. **F)** Mice (n = 4 per group) were treated with 0.75 U/kg BLM for 7 days after which lungs were harvested and single cell suspensions were analyzed via flow cytometry for AHR expression in the indicated cell subsets. **G through I)** Mice (n = 5 per group) were treated with 0.75 U/kg bleomycin or saline control (WT). Single cell suspensions were prepared from collagenase digested lung tissue at 7-days post bleomycin and CD11c+ cells were purified via magnetic bead isolation. Expression of the indicated transcripts was analyzed via qRT-PCR. All experiments shown are representative of at least three independent experiments, statistical significance was determined via ANOVA in panel A and C-E, or student's T-test in panels G-I (* = $p < 0.05$, ** = $p < 0.01$, *** = $p < 0.001$, **** = $p < 0.0001$).

Figure 2

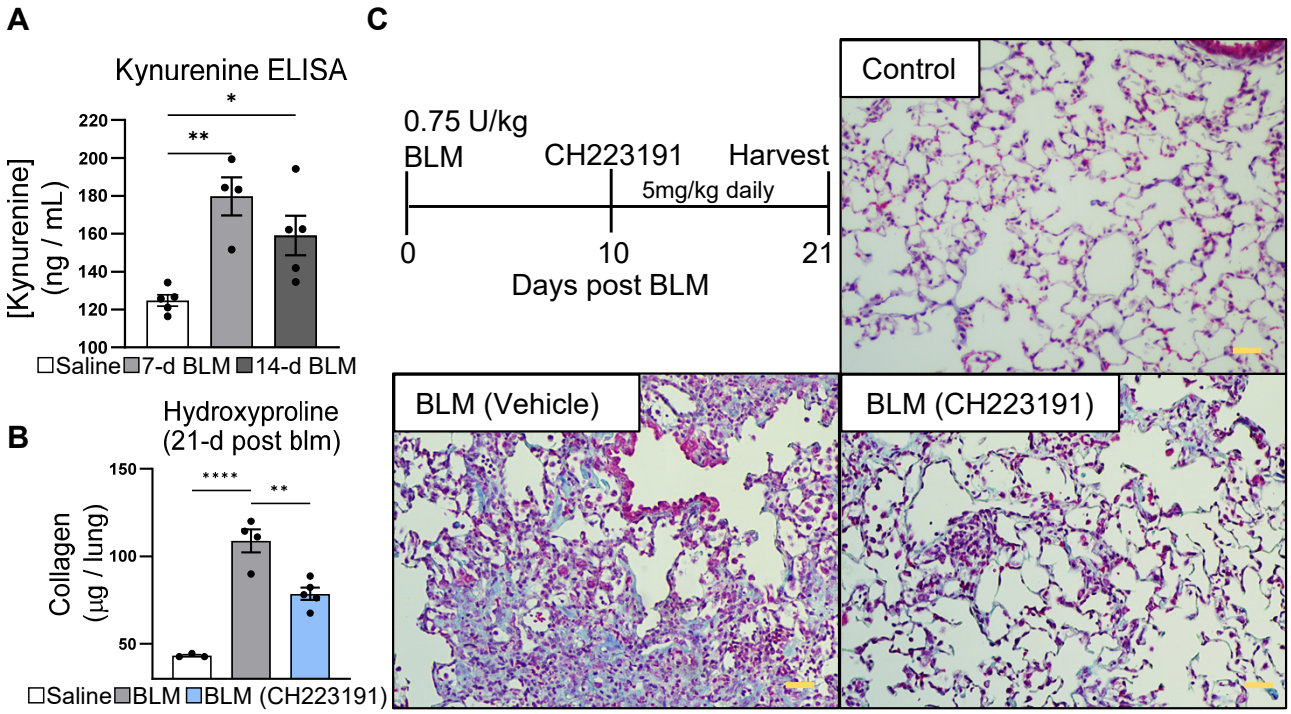

Figure 2. Production of AHR ligands is augmented during BLM induced fibrosis and complete AHR inhibition ameliorates disease. A) Mice (n = 4-5 mice per group) were treated with 0.75 U/kg BLM. Lungs were harvested at the indicated times and whole lung homogenates were assayed for KYN concentration by ELISA. **B)** Mice, (n = 3 – 5 per group) were treated with 0.75 U/kg bleomycin. Beginning at day 10 mice were treated daily with 5 mg/kg CH223191 dissolved in a vehicle of 2% Tween-20, 0.5% Carboxy methylcellulose, in PBS or vehicle alone by oral gavage until day 18. Lungs were harvested at Day 21 and lung collagen was quantified by hydroxyproline assay. **C)** Representative histology of lungs from B). Sections were stained with trichrome which highlights collagen fibers as blue staining (scale bar = 50 µM). All experiments shown are representative of at least three independent experiments, statistical significance was determined via ANOVA (* = $p < 0.05$, ** = $p < 0.01$, **** = $p < 0.0001$).

Figure 3

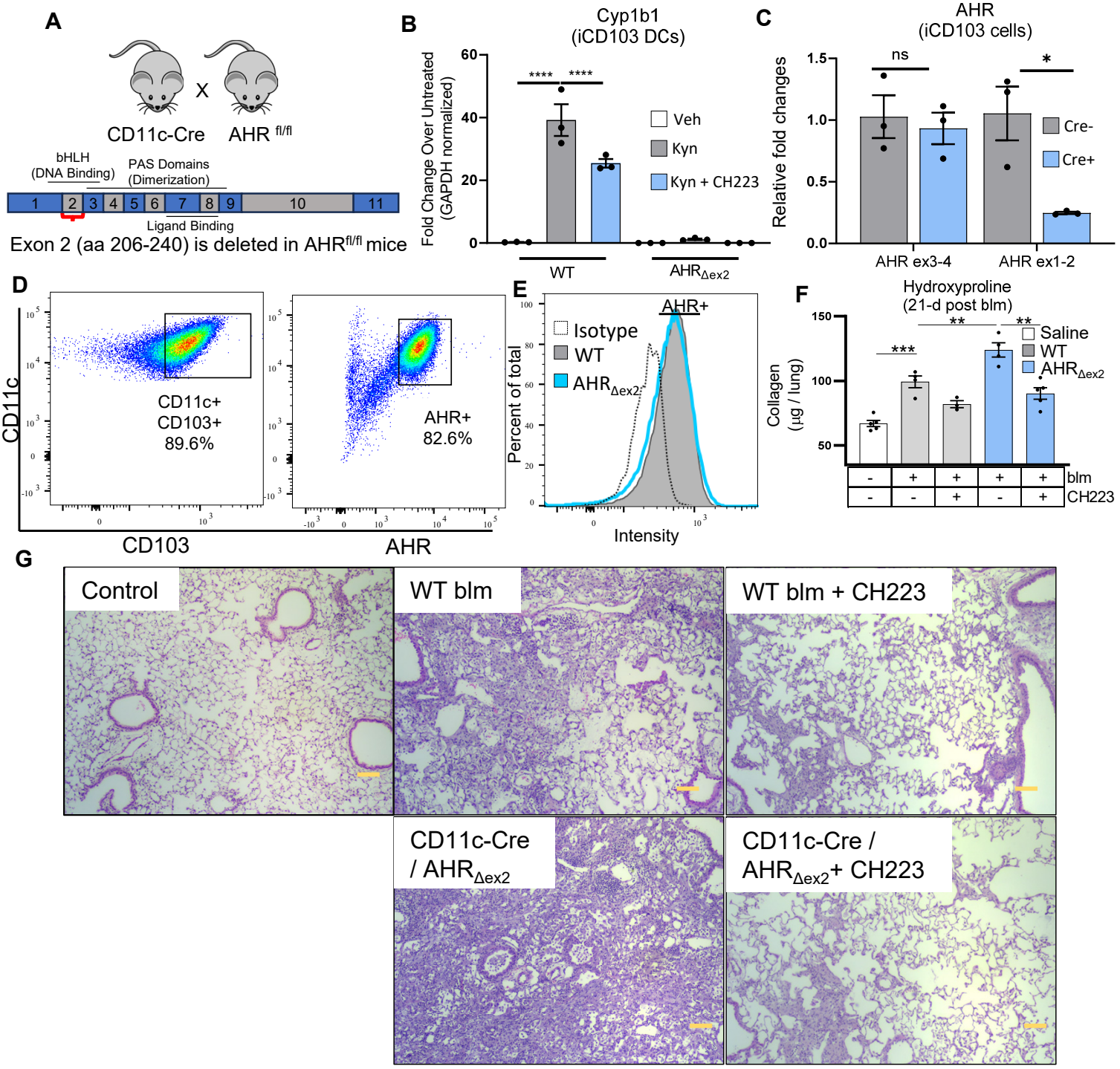

Figure 3. Deletion of AHR exon-2 reduces canonical AHR signaling in DCs but AHR expression is retained and augments inflammatory non-canonical AHR signaling. A) Cartoon schematic of murine AHR depicting the deletion of AHR exon-2 containing the DNA binding bHLH domain. Numbered boxes correlate to individual exons. **(B and C)** iCD103+ DCs were generated from WT B6 mice or $AHR_{\Delta ex2}$ mice and treated with 200 µM KYN or 10 µM CH223191 (CH223). 18 hours after treatment, RNA was harvested and expression of the canonical AHR gene Cyp1b1 (A) or AHR (B) was analyzed via qRT-PCR. **D)** iCD103+ DCs were analyzed via flow cytometry for expression of CD11c and CD103 as well as intracellular expression of AHR. **E)** Representative histogram showing AHR expression in WT or $AHR_{\Delta ex2}$ iCD103 DCs analyzed via flow cytometry. **F and G)** Mice (n = 5 per group) were treated with 0.75 U/kg bleomycin. At 10-d post bleomycin groups of mice were administered CH223191 (5 mg/kg) or vehicle alone daily until 18-d post bleomycin. Lungs were harvested at 21-d post bleomycin collagen content was quantified via hydroxyproline assay (F) and lung fibrosis was examined via histopathologic examination of fixed lung sections (A: Scale bar = 100 µM panel G). All experiments shown are representative of at least three independent experiments, statistical significance was determined via ANOVA in panel A or student's t-test in panel B (* = $p < 0.05$, ** = $p < 0.01$, **** = $p < 0.0001$).

Figure 4

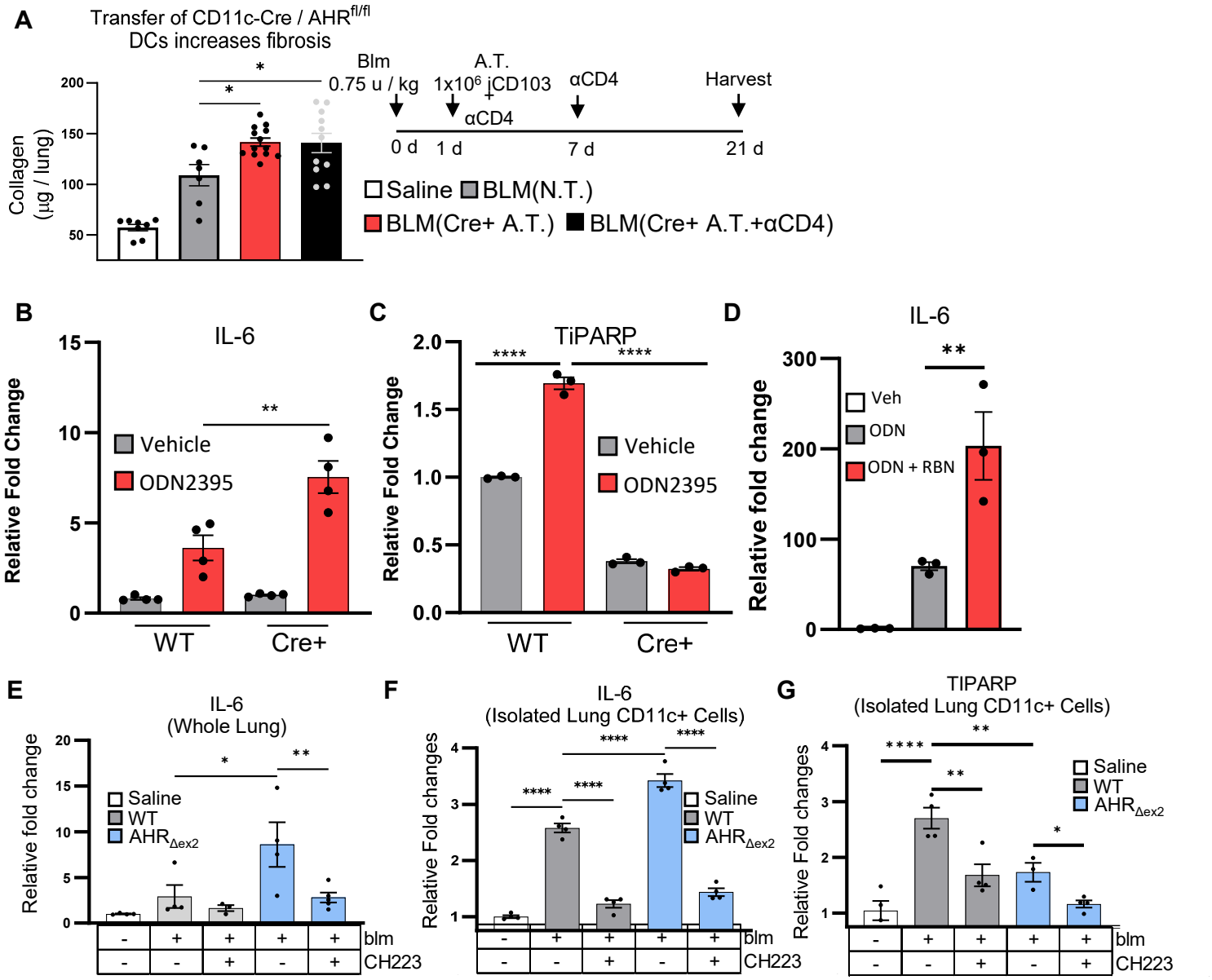

Figure 4. Loss of canonical AHR signaling in CD11c+ cells exacerbates fibrosis via a ncAHR dependent mechanism. A) Mice (n = 7 mice no transfer group and 11 mice Cre+ transfer groups) were treated with 0.75 U/kg bleomycin. At 1-d post-BLM 1x10^6 iCD103 cells generated from naïve CD11c-Cre+ AHR$_{\Delta ex2}$ mice were adoptively transferred via tail vein injection. Additionally, one group was administered 100 µg αCD4 neutralizing antibody at 1- and 7-d post bleomycin. Lungs were harvested 21-d post bleomycin and collagen content was quantified via hydroxyproline assay. **B through D)** iCD103 cells were generated as described. Cells were stimulated with 1 µM ODN2395 (TLR9 agonist), 10 µM RBN2397 (TiPARP inhibitor), or a vehicle control for 18 hours. Cells were harvested and RNA was analyzed for expression of IL-6 or TiPARP transcript via qRT-PCR. **E)** WT-B6 or AHR$_{\Delta ex2}$ mice were treated with 0.75 U/kg BLM, CH223191 (CH223) was administered from day 10- to 18-post BLM. Lungs were harvested at 21-day post BLM and expression of IL-6 transcript were quantified via qRT-PCR. **F and G)** Mice (n = 5 - 7 per group) were treated with 0.75 U/kg bleomycin or saline control (WT). Single cell suspensions were prepared from collagenase digested lung tissue at 7-days post bleomycin and CD11c+ cells were purified via magnetic bead isolation after which cells were pooled and treated overnight *ex-vivo* (n = 4 per group) with either 30µM CH223191 (CH223) or DMSO vehicle control. Expression of the indicated transcripts was analyzed via qRT-PCR. All experiments shown are representative of at least three independent experiments, statistical significance was determined via ANOVA (* = $p < 0.05$, ** = $p < 0.01$, *** = $p < 0.001$, **** = $p < 0.0001$).

Figure 5

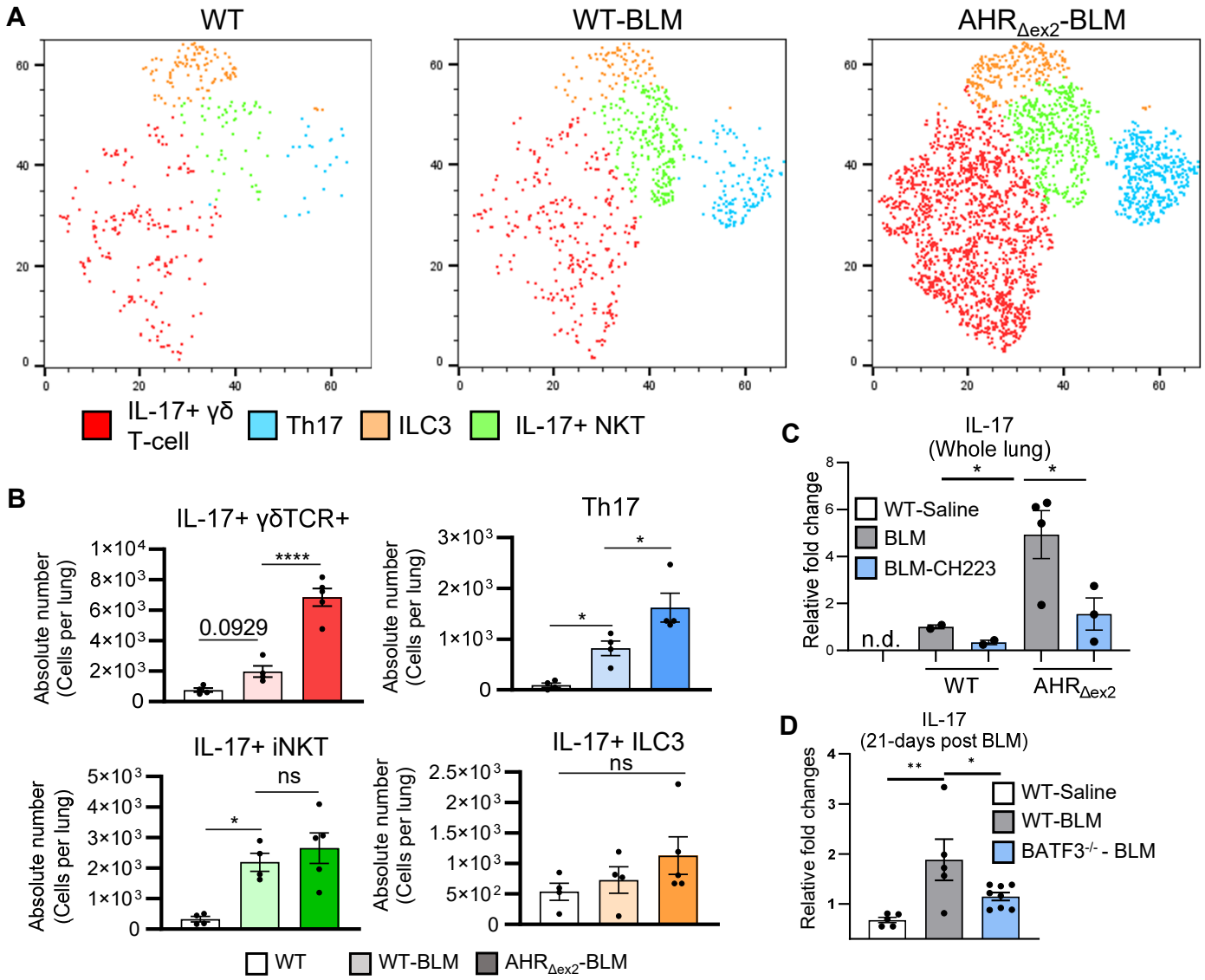

Figure 5. ncAHR signaling in CD11c+ cells drives IL-17 production in the lung. A) WT B6 or $AHR_{\Delta ex2}$ mice (n = 5 per group) were treated o.p. with 0.75 U/kg BLM. 7-days post-BLM lungs were harvested and lung leukocytes were analyzed by flow cytometry for the following populations Th17 (CD45+, Thy1.2+, CD3+, CD4+, IL-17A+), IL-17+ γδ t-cell (CD45+, Thy1.2+, CD3+, CD4-, γδ-TCR+, IL-17A+), IL-17+ ILC3 (CD45+, Thy1.2+, CD3-, CD4-, IL-17+), IL-17A+ iNKT (CD45+, Thy1.2+, CD4-, CD3+, γδ-TCR+, IL-17A+). **B)** Quantification of cell populations identified in A. **C)** WT-B6 or $AHR_{\Delta ex2}$ mice were treated with 0.75 U/kg BLM, CH223191 (CH223) was administered from day 10- to 18-post BLM. Lungs were harvested at 21-day post BLM and expression of IL-17 transcript was quantified via qRT-PCR. **D)** Mice (n = 5-8 per group) were treated with 0.75 U/kg BLM. 21-days post BLM treatment, lungs were harvested and expression of IL-17 transcript from whole lung was analyzed via qRT-PCR. All experiments shown are representative of at least three independent experiments, statistical significance was determined via ANOVA (* = $p < 0.05$, ** = $p < 0.01$, **** = $p < 0.0001$).

Figure 6

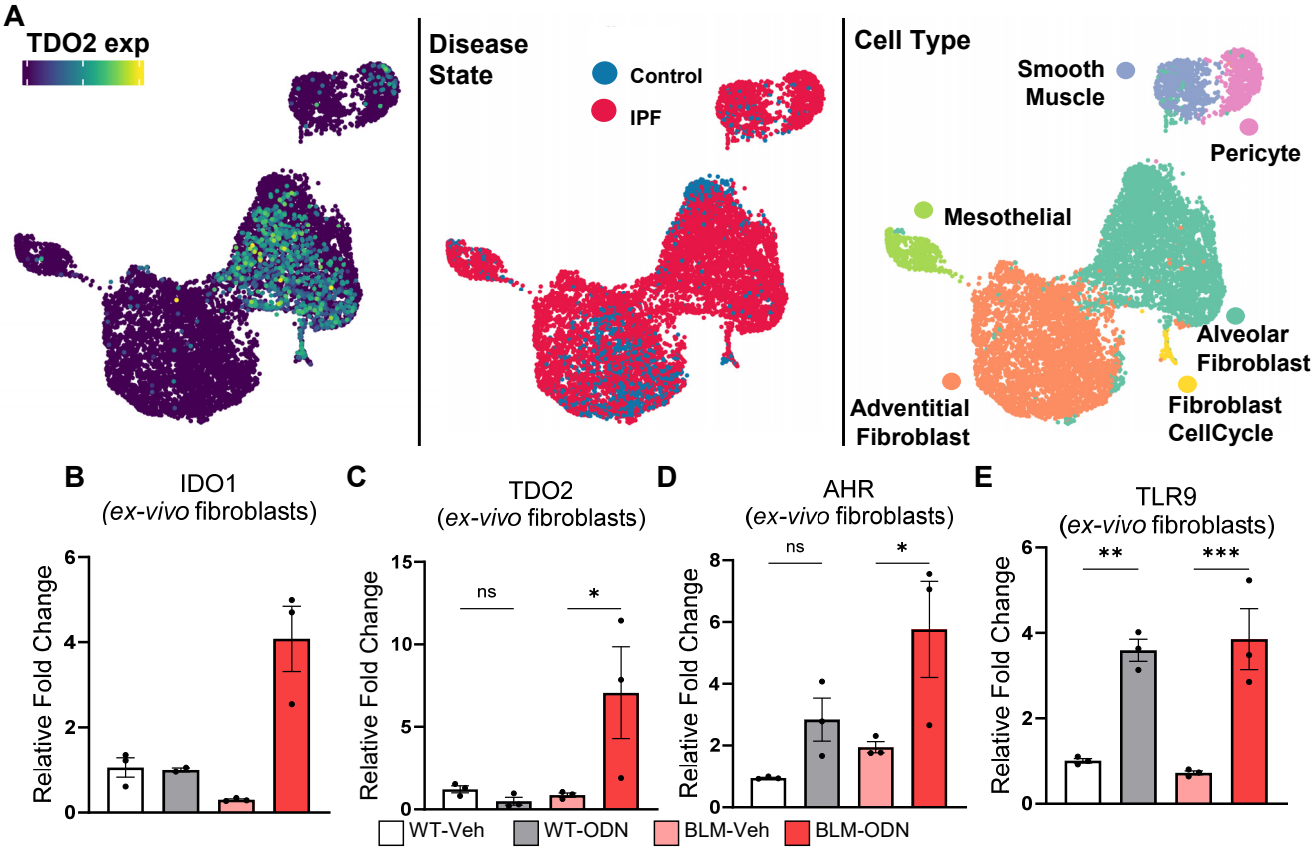

Figure 6. Fibroblasts isolated from fibrotic individuals express the kynurenine pathway enzymes IDO and TDO in response to TLR9 stimulation. A) Uniform manifold approximation and projections (UMAPs) of human lung stromal cells labeled by normalized expression of TDO2, cell type, and disease. **B through E**) Lung fibroblasts were cultured from groups of mice treated with BLM for 21-d or untreated as control. Fibroblasts were subsequently treated with the TLR9 agonist ODN2395 (ODN) or vehicle control (veh) for 18-h. Expression of the indicated transcript was analyzed via qRT-PCR. All experiments shown are representative of at least two independent experiments, statistical significance was determined via ANOVA (* = $p < 0.05$, ** = $p < 0.01$, *** = $p < 0.001$).

Figure 7

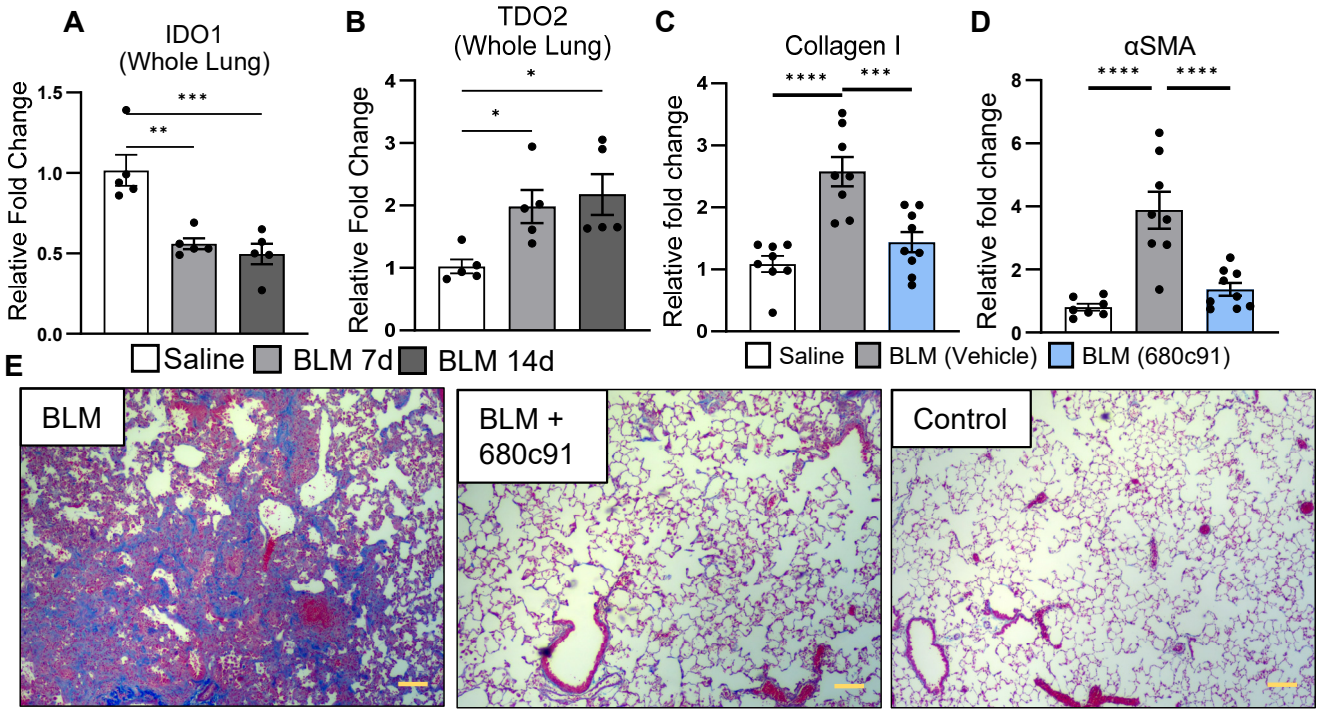

Figure 7. Inhibition of TDO2 rescues BLM induced fibrosis. (A and B) Groups of mice (n = 5 per group) were treated with 0.75 U/kg BLM or saline control for 7-14 days after which expression of the indicated transcript was analyzed in whole lung via qRT-PCR. **(C and D)** Group of mice (n = 8 – 9 per group) were treated with 0.75 U/kg BLM or saline control. Beginning on day 10 one group was treated with 15 mg/kg TDO2 inhibitor (680C91) daily by oral gavage until day 18 after which lungs were harvested and expression of the indicated transcript was assayed via qRT-PCR. **(E)** Representative histology (n =2 mice per group) showing assessment of collagen deposition by trichrome staining (blue staining) scale bar represents 100μm. All experiments shown are representative of at least two independent experiments, statistical significance was determined via ANOVA (* = $p < 0.05$, ** = $p < 0.01$, *** = $p < 0.001$).

Figure 8

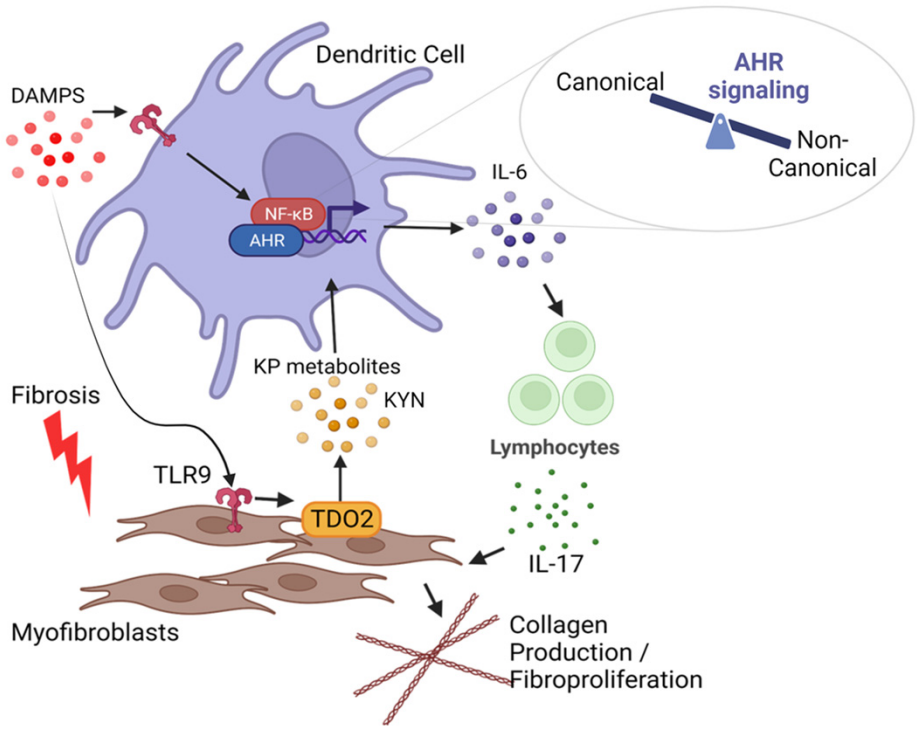

Figure 8. Working model for how fibroblast DC crosstalk contributes to fibrosis. Myofibroblasts express the kynurenine pathway enzyme TDO2 in response to TLR9 stimulation. kynurenine pathway metabolites active ncAHR signaling in DCs which, in cooperation with inflammatory TLR singling, augments production of IL-6 resulting in production of IL-17 from lymphocytes. Fibroblasts can be directly activated by IL-17 resulting in collagen production and fibroproliferation.